

# Maximal Causes for Exponential Family Observables

S. Hamid Mousavi, Jakob Drefs, Florian Hirschberger, Jörg Lücke

Machine Learning Lab, Department of Medical Physics and Acoustics  
University of Oldenburg, Germany

## Abstract

Latent variable models represent observed variables as parameterized functions of a set of latent variables. Examples are factor analysis or probabilistic sparse coding which assume weighted linear summations to determine the mean of Gaussian distribution for the observables. However, in many cases observables do not follow a normal distribution, and a linear summation of latents is often at odds with non-Gaussian observables (e.g., means of the Bernoulli distribution have to lie in the unit interval). Furthermore, the assumption of a linear summation model may (for many types of data) not be closely aligned with the true data generation process even for Gaussian observables. Alternative superposition models (i.e., alternative links between latents and observables) have therefore been investigated repeatedly. Here we show that using the maximization instead of summation to link latents to observables allows for the derivation of a very general and concise set of parameter update equations. Concretely, we derive a set of update equations that has the same functional form for all distributions of the exponential family. Our results consequently provide directly applicable learning equations for commonly as well as for unusually distributed data. We numerically verify our analytical results assuming standard Gaussian, Gamma, Poisson, Bernoulli and Exponential distributions. We point to some potential applications by providing different experiments on the learning of variance structure, noise type estimation, and denoising.

*Keywords:* Sparse coding, exponential family distributions, expectation maximization, variational lower bound.

## 1 Introduction

Probabilistic Principle Component Analysis (p-PCA) [1, 2], Factor Analysis (FA) [3] or Sparse Coding (SC) [4] are well-known latent variable approaches which seek to model observable distributions, and are used to extract latent information from data. The data models of these approaches consist of latent variables whose weighted linear sum determines the mean of a Gaussian distribution. In probabilistic sparse coding, for instance, the set of  $D$  observed variables  $y_d$  is modelled by a set of  $H$  latent variables  $s_h$  according to the following generative model:

$$p(\vec{s} | \Theta) = \prod_{h=1}^H p_{\text{sparse}}(s_h; \Lambda) \quad (1)$$

$$p(\vec{y} | \vec{s}, \Theta) = \prod_{d=1}^D \mathcal{N}(y_d; \sum_{h=1}^H W_{dh} s_h, \sigma^2) \quad (2)$$

where  $\vec{W}_h = (W_{1h}, \dots, W_{Dh})^T$  is commonly referred to as the *generative field* of unit  $h$ . The matrix containing all generative fields,  $W = (\vec{W}_1, \dots, \vec{W}_H)$ , is commonly referred to as the model’s *dictionary*. Here,  $\Theta = (\Lambda, W, \sigma^2)$  denotes all parameters of the model and the term ‘ $p_{\text{sparse}}$ ’ refers to a sparse distribution that is used as prior distribution  $p(\vec{s} | \Theta)$ . The canonical choice for such a distribution is the Laplace distribution (see, e.g., [4, 5]). Other choices include the Cauchy distribution (which was used by [4], alongside Laplace), student-t [6], Bernoulli [7, 8], categorical [9], or spike-and-slab [10, 11, 12].

Sparse coding is a standard and active field of research with a high relevance for computational neuroscience and tasks such as feature learning, denoising, inpainting, compression and compressive sensing [13, 14]. Furthermore, the theory of sparse coding has close links to deep learning approaches (e.g. [15]). The predominant approaches to infer the generative fields  $W$  are deterministic algorithms which exploit the specific form of (1) and (2). The Lasso approach [5], for instance, is based on a maximum-a-posteriori (MAP) estimate of the latent vector  $\vec{s}$  (whose elements are taken to be Laplace distributed). Given the data points  $\vec{y}$ , the corresponding MAP estimate  $\vec{s}$  can then be computed (approximately) by solving a convex optimization problem. Given the MAP estimates, the  $W$  matrix is updated using standard closed-form updates for  $W$ , see for instance [4, 5]. MAP approaches are less suitable for sparse coding models that use priors with richer structure (e.g. [6, 10]) where approximate inference approaches such as sampling or variational optimization are applied instead. For many types of data, the generative fields inferred by standard sparse coding have been interpreted as structural primitives of the corresponding data [16]. Presumably most prominently, the generative fields inferred from whitened image patches have been linked to edges [4].

Not all data is subject to Gaussian noise, however, and the linear superposition of generative fields does often not reflect the true generative process of the data well. In fact, it has been argued, e.g., for images [17] or for cochlear representations of sounds [18, 19, 20], that a linear superposition model is difficult to motivate. Consequently non-linear as well as non-Gaussian generalizations have previously been of interest.

Generalizations to non-linear superposition models have, for instance, been investigated in the form of non-linear Independent Component Analysis (ICA) [21, 22, 23]. We can regard standard ICA as a noiseless limit of standard sparse coding [24]. The practical realizations of non-linear ICA make use of a post-linear non-linearity (i.e., a linear superposition followed by a sigmoidal non-linearity). Other lines of research investigate non-linearities in the form of a maximum in place of the sum [18, 19, 25, 20].

Likewise, latent variable approaches for non-Gaussian observation noise have been of considerable interest. Related work includes factor analysis with Poisson noise [26], PCA with Poisson noise [27], exponential family PCA (EF-PCA) [28, 29], and non-negative matrix factorization, where non-Euclidean distances are frequently used (see, e.g., [30] and references therein). Furthermore, sparse coding with exponential family noise has been investigated previously [31]. We will elaborate on these approaches further below.

Notably, most approaches considered so far, either focused on changing the non-linearity in sparse coding (like non-linear ICA [21, 22, 23] or Maximal Causes Analysis (MCA) [32, 25]) or the noise model (like EF-PCA [28] or exponential family sparse coding [31]). An exception is an early combination of the maximum non-linearity together with a Poisson noise model [19] (although further developments for efficient training [32] dropped back to Gaussian noise). Latent variable approaches such as noisy-OR Bayes nets with sparse binary activations [33, 34], Boolean Factor Analysis (BFA) [35] or shallow Sigmoid Belief Networks (SBN) [36, 37] could, furthermore, be considered as sparse coding models with Bernoulli noise and specific non-linear superposition (in the form of noisy-OR non-linearity or in the form of a post-linear superposition for SBNs; also

compare approaches such as [38]).

A central challenge for all latent variable models with non-Gaussian observables and/or non-linear superposition is the derivation of parameter update equations. Here, we replace the weighted summation over latents by a maximization (compare [18, 19]). Using this maximum superposition, we show that exceptionally general and concise update equations are obtained that are directly applicable to any member of the exponential family; and, as potential examples, we further provide numerical evaluations for one- as well as two-parameter distributions. At the same time, the used model family maintains the standard coupling of latents to observables in the sense that the superposition model always sets the *mean* of the observable distribution, i.e., unlike previous approaches the superposition model does not change with the used observable distribution.

## 2 A Family of Non-Linear Sparse Coding Models

We will first define the family of generative models we seek to optimize. We will use noise distributions  $p(y; \vec{\eta})$  of the exponential family given by:

$$p(y; \vec{\eta}) = h(y) \exp(\vec{\eta}^T \vec{T}(y) - A(\vec{\eta})), \quad y \in \mathcal{Y} \quad (3)$$

where  $\mathcal{Y}$  is the domain of the observables,  $h(y)$  is the base measure,  $\vec{T}(y)$  represents the *sufficient statistics* of the data, and  $\vec{\eta}$  and  $A(\vec{\eta})$  are *natural parameters* and *log-partition*, respectively. The vectors  $\vec{T}(y) = (T_1(y), \dots, T_L(y))^T$  and  $\vec{\eta} = (\eta_1, \dots, \eta_L)^T$  have  $L$  elements each when distribution  $p(y; \vec{\eta})$  is an  $L$ -parameter distribution.

As an important tool to later derive parameter update equations, we will use the *mean value parameterization* of the exponential family (e.g. [39, 40]), i.e., we will consider parameters  $\vec{w} = (w_1, \dots, w_L)^T$  defined by

$$\vec{w} := \langle \vec{T}(y) \rangle_{p(y; \vec{\eta})} \quad (4)$$

where  $\langle f(y) \rangle_{p(y)}$  denotes the expectation value of  $f(y)$  w.r.t. the distribution  $p(y)$  (evaluated per entry if  $f$  is a vector). Instead of  $\langle f(y) \rangle_{p(y)}$  an alternative notation would be using  $\mathbb{E}_p[f(y)]$ . However, we will use the former notation in the following for the sake of consistency with previous works [19, 12].

The mapping (4) is bijective and its inverse is well defined in non-degenerate cases<sup>1</sup>. Assuming invertibility from now on, there exists a function  $\vec{\Phi}$  which maps the mean value parameters to the natural parameters,

$$\vec{\eta} = \vec{\Phi}(\vec{w}), \quad \text{such that} \quad \vec{w} = \langle \vec{T}(y) \rangle_{p(y; \vec{\Phi}(\vec{w}))} \quad (5)$$

Let us now consider a set of  $N$  data points,  $Y = \{\vec{y}^{(1)}, \dots, \vec{y}^{(N)}\}$  where each datum  $\vec{y}^{(n)}$  is a vector with  $D$  entries. As latent variables  $\vec{s}$  we consider  $H$  dimensional vectors with binary entries,  $s_h \in \{0, 1\}$ . Concrete example algorithms will (for simplicity) assume these latents to be distributed according to  $H$  independent Bernoulli distributions. The analytical results derived in the following will, however, also apply for general binary latents  $\vec{s}$ . They could hence also be used in conjunction with more complex priors, e.g., priors given by deep models with binary variables

<sup>1</sup>Essentially the mapping is invertible when the elements of  $\vec{T}(y)$  are not interdependent (compare [39]). A counter-example is, for instance, the beta distribution with parameters  $\alpha = \beta$ . Also see *minimal representation* property [41].

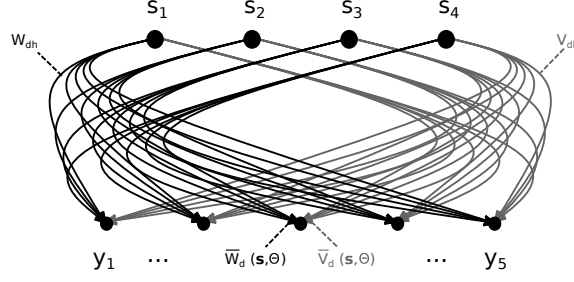


Figure 1: Proposed generative model with  $H = 4$  hidden variables and  $D = 5$  observed variables. Given a set of binary vector  $\vec{s}$ , the value  $y_d$  of the observables is conditionally independent and drawn from any of the exponential family distributions with mean value parameters  $\bar{W}_d$  and  $\bar{V}_d$  determined by weights  $W_{1d}, \dots, W_{4d}$  and  $V_{1d}, \dots, V_{4d}$ , respectively.

such as SBNs, noisy-OR and so forth. As for standard sparse coding, we assume all observables to be distributed equally but allow for any distribution of the exponential family:

$$p(\vec{s} | \Theta) = \prod_h \pi_h^{s_h} (1 - \pi_h)^{1-s_h} \quad (6)$$

$$p(\vec{y} | \vec{s}, \Theta) = \prod_d p(y_d; \vec{\eta}_d(\vec{s}, \Theta)), \quad \text{where} \quad (7)$$

$$p(y; \vec{\eta}) = h(y) \exp(\vec{\eta}^T \vec{T}(y) - A(\vec{\eta})) \quad (8)$$

and where  $\Theta$  denotes the parameters of the model. For model (6) to (8), the latent variables  $\vec{s}$  couple to the observed variable  $y_d$  through the function  $\vec{\eta}_d(\vec{s}, \Theta)$  which is defined further below (the function can be considered as a link function in a broader sense, we elaborate in Appendix A). Note that  $\vec{\eta}_d(\vec{s}, \Theta)$  is a vector with  $L$  entries for each  $d = 1, \dots, D$ . For standard sparse coding, the latents set the *mean* of the observables using a matrix  $W \in \mathbb{R}^{D \times H}$ . Here we will seek to couple latents and observables in an analog but more generally applicable way. To facilitate our notation, let us assume two-parameter distributions from now on ( $L = 2$ ) as applies, e.g., for Gaussian or Gamma distributions. Arbitrary  $L$  will be treated later on. For the  $L = 2$  case, the mean value parameters  $\vec{w}$  (Eqns. 4 and 5) will be denoted by  $w_1 = \bar{W}$  and  $w_2 = \bar{V}$ . The notation serves for gaining some intuition because, e.g., for Gaussian or Gamma distributions,  $\bar{W}$  can be thought of as the parameter of the mean, and  $\bar{V}$  as the parameter of the variance (or of the second moment). We require parameters  $\bar{W}$  and  $\bar{V}$  for each observable, and they will depend on the latents  $\vec{s}$  and two  $D \times H$  matrices  $W$  and  $V$ . Fig. 1 then illustrates the structure of the proposed model. Using the function  $\vec{\Phi}(\vec{w})$  of (5) we now define the link from latents to observables as follows:

$$\vec{\eta}_d(\vec{s}, \Theta) := \vec{\Phi}(\bar{W}_d(\vec{s}, \Theta), \bar{V}_d(\vec{s}, \Theta)), \quad d = 1, \dots, D. \quad (9)$$

**Example 1:** To provide intuition for the link defined by (9) consider Gaussian observation noise. In the Gaussian case sufficient statistics and natural parameters are given by  $\vec{T} = (y, y^2)^T$  and  $\vec{\eta} = (\frac{\mu}{\sigma^2}, \frac{-1}{2\sigma^2})^T$  (where  $\mu$  and  $\sigma^2$  are the mean and variance of the Gaussian distribution, respectively). By expressing the mean value parameters  $\vec{w}$  in terms of the natural parameters  $\vec{\eta}$ , we get:

$$\vec{w} = \begin{pmatrix} \mu \\ \mu^2 + \sigma^2 \end{pmatrix} = \frac{1}{4\eta_2^2} \begin{pmatrix} -2\eta_1\eta_2 \\ \eta_1^2 - 2\eta_2 \end{pmatrix}. \quad (10)$$

Based on the equation (10), the inverse mapping  $\vec{\Phi}$  can be computed in closed-form (in this case) and is given by:

$$\vec{\Phi}(\vec{w}) = \frac{1}{2(w_2 - w_1^2)} \begin{pmatrix} 2w_1 \\ -1 \end{pmatrix}. \quad (11)$$

By using definition (9), the coupling of latents to observable is consequently given by:

$$\begin{aligned} \vec{\eta}_d(\vec{s}, \Theta) &= \vec{\Phi}(\bar{W}_d(\vec{s}, \Theta), \bar{V}_d(\vec{s}, \Theta)) \\ &= \frac{1}{2(\bar{V}_d(\vec{s}, \Theta) - \bar{W}_d^2(\vec{s}, \Theta))} \begin{pmatrix} 2\bar{W}_d(\vec{s}, \Theta) \\ -1 \end{pmatrix}. \end{aligned} \quad (12)$$

In order to recover standard linear sparse coding, we can complete the definition of  $\vec{\eta}_d$  as follows. Using parameters  $\Theta = (\sigma^2, W)$  with  $\sigma^2 \in \mathbb{R}^+$  and  $W \in \mathbb{R}^{D \times H}$  we define:

$$\bar{W}_d(\vec{s}, \Theta) = \sum_h W_{dh} s_h \quad \text{and} \quad \bar{V}_d(\vec{s}, \Theta) = \sigma^2 + \bar{W}_d^2(\vec{s}, \Theta). \quad (13)$$

This results in:

$$\vec{\eta}_d(\vec{s}, \Theta) = \begin{pmatrix} (W\vec{s})_d / \sigma^2 \\ -1/2\sigma^2 \end{pmatrix} \quad (14)$$

i.e., we recover the standard sparse coding parameterization with  $\mu_d = (W\vec{s})_d$  as the mean of observable  $d$  and  $\sigma^2$  as its variance (with  $\sigma^2$  being the same for all  $d$ ).  $\square$

**Relation to previous work.** Gaussian distributions do not model many types of data well. It has therefore been the goal of many previous latent variable models to generalize learning algorithms developed for the Gaussian case to other distributions or to exponential family distributions [28, 29, 31, 42, 43, 44, 45, 26, 27]. As an important reference for this work, the approach of exponential family sparse coding (EF-SC) [31] defines a sparse coding approach for noise distributions of the exponential family. The work chooses a link function that assumes the natural parameters of an exponential family distribution to be given by a linear superposition of generative fields. Essentially, if  $\tilde{\eta}_d(\vec{s}, \Theta)$  is the natural parameter of a one-parameter distribution, then  $\tilde{\eta}_d(\vec{s}, \Theta) = (W\vec{s})_d$  (in [31]  $W$  is denoted by  $B$ ). With a link defined in this way and a standard Laplacian prior, the posteriors of the model maintain a mono-modal shape such that a maximum a-posteriori (MAP) approximation can be applied [31]. However, MAP-based training of sparse coding is usually restricted to the generative fields; like for standard sparse coding, neither the prior parameters nor the parameters of the noise model are inferred. Cross-validation may be used in addition but is only feasible for very few additional parameters. Furthermore, setting the natural parameters of a given exponential family distribution using a linear superposition may (while mathematically convenient) not capture the true data generation process well. Depending on the distribution, a linear superposition may divert substantially from the standard choice of setting the distribution mean. If we use Poisson noise as a simple one-parameter example, then the natural parameters are given by  $\eta = \log(\lambda)$ , where  $\lambda$  is the mean. Exponential family sparse coding according to [31]

would then use  $\lambda_d = \exp(\sum_h W_{dh}s_h)$  for an observable  $d$ . The same choice of coupling was used more recently for the Poisson PCA approach [27] which does focus on Poisson noise and reported state-of-the-art denoising performance when it was first suggested (also see [44]). Other distributions of the exponential family will result in other types of non-linearities if the natural parameters are assumed to be set by a linear sum.

Exponential family sparse coding (EF-SC) [31] and Poisson PCA [27] both borrow their link from latents to observables from the previously investigated exponential family PCA (EF-PCA) approach [28]. In addition to the same link, EF-PCA uses (like Poisson PCA) a deterministic optimization for parameter learning. The original EF-PCA work only considered one-parameter distributions of the exponential family with sufficient statistics proportional to  $x$  ([28], Eqn. 2), which would exclude the Pareto, Laplace and other one-parameter distributions. A fully Bayesian approach to exponential family PCA [29] also uses the linear superposition to set the natural parameters but replaces MAP-based learning with a Hybrid Monte Carlo approach (which allows for also learning parameters other than the weight matrix). Bayesian EF-PCA is formulated for distributions of the exponential family with one and several parameters but the concrete algorithm uses a sufficient statistics equal to the identity function ([29], Eqn. 7). EF-SC [31] is more general in its initial formulation. However, the generative fields that are used are all defined to set one-parameter distributions (their matrix  $B$  sets the natural parameter of an exponential family distribution). Also for the Gaussian case, which is used as an introductory example, a single-parameter Gaussian (with known variance) is chosen. Notably, none of the above mentioned previous approaches (i.e., Poisson PCA [27], Poisson factor analysis [26], EF-PCA [28], Bayesian EF-PCA [29] and EF-SC [31]) used any other than one-parameter distributions of the exponential family in their contributions. Moreover, and to our best knowledge, the numerical experiments of those contributions (including EF-SC) only used two specific one-parameter distributions: Bernoulli and Poisson. Although, e.g. EF-SC, would in principle be able to treat other distributions, the meaning of setting all natural parameters using a linear superposition of latents is arguably unclear. For instance, even for a Gaussian (as a standard two-parameter distribution) the second moment would be determined by two linear sums. Such a case (and more intricate cases resulting from other two-parameter distributions) have not been discussed or treated by these approaches. One example of a study which did investigate other than the Bernoulli and Poisson distribution is work by Khan et al. [46] where a generalized mixture of factor analyzers model is presented that cope with both continuous and discrete data (Gaussian and Multinomial distributions have been treated). Further, a new variational EM algorithm is established in this contribution based on a lower bound of the Multinomial likelihood for fitting the model to the considered mixed data. Although the model can, in principle, deal with binary and categorical data along with the continuous case, it is not defined to subsume all distributions of the exponential family.

In addition, note that approaches such as EF-SC are, furthermore, restricted in other aspects of learning. As a deterministic MAP-based learning is used, only weight parameters are updated (and neither additional noise nor prior parameters). In summary, it may thus be argued that no latent variable model can be applied (both in theory and for practical optimizations) to the whole exponential family. Once a model is defined, the challenge is, of course, the derivation of a general parameter optimization procedure. Here we address the goal of model definition and parameter optimization using a non-linear superposition model to couple latents to observables. All approaches discussed above maintain a linear superposition assumption; and when a general formulation for the exponential family is aimed at, the Gaussian case is generalized by using the linear superposition to set the natural parameters. For the here used non-linear superposition can also be seen as a generalization of the Gaussian case but we will maintain that the used superposition sets the mean of a given observable distribution. Notably, for the specific choice of the Poisson distribution, approaches such as Poisson Factor Analysis [26] also have chosen to

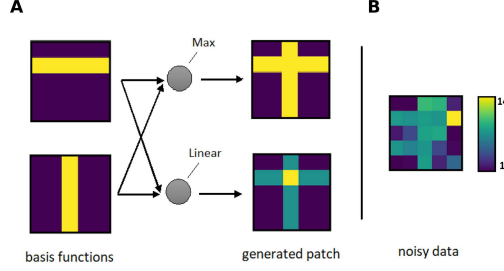


Figure 2: Illustration of non-linear versus linear combination of generative fields. **A** Two arbitrary basis functions that combined through maximum and linear combinations to generate data. **B** A noisy datapoint obtained from the max superposition of the two basis functions plus Exponential noise.

couple the latents to the mean of the distribution rather than to its natural parameter. For our non-linear superposition, we will also keep such a coupling to the distribution mean but the coupling will be defined for the general case.

**Non-linear Superposition Model.** In Example 1, given a matrix  $W \in \mathbb{R}^{D \times H}$ , the mean  $\mu_d$  of observable  $d$  was given by  $(W\vec{s})_d$ . Our definition of the link from latents to observables (9) is sufficiently flexible to also allow for other types of superpositions that can be defined by the functions  $\bar{W}_d(\vec{s}, \Theta)$  or  $\bar{V}_d(\vec{s}, \Theta)$ . In this respect the question arises what aspects of a given observable distribution the two functions shall determine. Most commonly the latents determine the *mean* of observable  $d$  using (e.g., for p-PCA, sparse coding etc). For many members of the exponential family, the first mean value parameter coincides with the mean of the corresponding exponential family distribution (that is we have  $T_1(y) = y$ ). If this is the case, the function  $\bar{W}_d(\vec{s}, \Theta)$  alone directly determines the observable mean:

$$\begin{aligned} \mu_d &= \langle y \rangle_{p(y; \Phi(\bar{W}_d(\vec{s}, \Theta), \bar{V}_d(\vec{s}, \Theta)))} \\ &= \langle T_1(y) \rangle_{p(y; \Phi(\bar{W}_d(\vec{s}, \Theta), \bar{V}_d(\vec{s}, \Theta)))} = \bar{W}_d(\vec{s}, \Theta) \end{aligned} \quad (15)$$

where the last step follows from (5). The function  $\bar{W}_d(\vec{s}, \Theta)$  can then be chosen as a linear superposition  $\bar{W}_d(\vec{s}, \Theta) = (W\vec{s})_d$  as in Example 1 or as a non-linear superposition. Here, we will follow previous work [19, 17, 20] and demand that the mean of a given observable distribution is given by the maximum instead of the sum. More concretely, we will replace (e.g., for the Gaussian or Gamma distribution):

$$\bar{W}_d(\vec{s}, \Theta) = (W\vec{s})_d = \sum_h W_{dh} s_h \quad \text{by} \quad \bar{W}_d(\vec{s}, \Theta) = \max_h \{W_{dh} s_h\}. \quad (16)$$

Fig. 2 illustrates the differences between a maximum and a linear superposition of the latents using artificial bars. The maximum superposition has been suggested before for acoustic data [18, 19, 20] and for visual data [17] where it aligns more closely with the actual data generation process. At the same time, and importantly for the purposes of this paper, the specific properties of the maximum function will enable derivations of a generally applicable update procedure for any noise models of the exponential family.

Equation (16) would cover members of the exponential family such as Gaussian, Gamma etc (as  $T_1(y) = y$  holds for these distributions). However, to be applicable to the whole exponential family, the definition of the maximum superposition has to be generalized. The challenge is

that, in general, the sufficient statistics  $\vec{T}(y)$  may not have an element that is proportional to  $y$  (the Beta-distribution is one example where  $T_1(y) = \log(y)$  and  $T_2(y) = \log(1 - y)$ ). As a consequence, the definition of the maximum superposition has to involve both functions  $\bar{W}_d(\vec{s}, \Theta)$  and  $\bar{V}_d(\vec{s}, \Theta)$ . Nevertheless, it will be possible to define  $\bar{W}_d(\vec{s}, \Theta)$  and  $\bar{V}_d(\vec{s}, \Theta)$  such that the mean of the observables is determined by a maximum superposition. For this purpose consider a matrix  $M(\Theta) \in \mathbb{R}^{D \times H}$  which can potentially be a non-trivial function of the parameters  $\Theta$ . Given a latent vector  $\vec{s}$ , we now demand that the mean  $\mu_d$  of an observable  $d$  is given by:

$$\mu_d = \langle y \rangle_{p(y; \vec{\Phi}(\bar{W}_d(\vec{s}, \Theta), \bar{V}_d(\vec{s}, \Theta)))} \stackrel{!}{=} \max_h \{M_{dh}(\Theta) s_h\}. \quad (17)$$

Clearly, if  $T_1(x) = x$ , we can satisfy the demand by choosing  $\bar{W}_d(\vec{s}, \Theta) = \max_h \{W_{dh} s_h\}$ , which follows from (15):

$$\mu_d = \langle y \rangle_{p(y; \vec{\Phi}(\bar{W}_d(\vec{s}, \Theta), \bar{V}_d(\vec{s}, \Theta)))} = \bar{W}_d(\vec{s}, \Theta) = \max_h \{W_{dh} s_h\}. \quad (18)$$

Hence, in this case,  $M_{dh}(\Theta) = W_{dh}$ .

A definition of  $M(\Theta)$  which is generally applicable for the whole exponential family has to be more elaborate. So far, our derivation relied on the sufficient statistics  $T_1(y)$  being equal to  $y$ . For the general case, let us first define a matrix  $M(\Theta)$  before we show that it fulfills (17). We consider (as part of the model parameters  $\Theta$ ) two matrices  $W, V \in \mathbb{R}^{D \times H}$  and define  $M(\Theta) \in \mathbb{R}^{D \times H}$  as follows:

$$\forall d, h: M_{dh}(\Theta) = F(W_{dh}, V_{dh}) \quad \text{where} \quad F(w, v) = \langle y \rangle_{p(y; \vec{\Phi}(w, v))}. \quad (19)$$

Using matrix  $M(\Theta)$  we can now define our mappings  $\bar{W}_d(\vec{s}, \Theta)$  and  $\bar{V}_d(\vec{s}, \Theta)$  as follows:

$$\bar{W}_d(\vec{s}, \Theta) := W_{dh(d, \vec{s}, \Theta)}, \quad \bar{V}_d(\vec{s}, \Theta) := V_{dh(d, \vec{s}, \Theta)}, \quad (20)$$

$$\text{where} \quad h(d, \vec{s}, \Theta) := \operatorname{argmax}_h \{M_{dh}(\Theta) s_h\}.$$

That is, we define the functions  $\bar{W}_d(\vec{s}, \Theta)$  and  $\bar{V}_d(\vec{s}, \Theta)$  via an index  $h(d, \vec{s}, \Theta)$  which selects for a given observable  $d$  the latent with the maximal value of  $M_{dh}(\Theta)$ . Definitions (19) and (20) represent a generalization of the superposition model (18) suitable for the whole exponential family. To see this we derive:

$$\begin{aligned} \mu_d &= \langle y \rangle_{p(y; \vec{\eta}_d(\vec{s}, \Theta))} = \langle y \rangle_{p(y; \vec{\Phi}(\bar{W}_d(\vec{s}, \Theta), \bar{V}_d(\vec{s}, \Theta)))} \\ &= F(\bar{W}_d(\vec{s}, \Theta), \bar{V}_d(\vec{s}, \Theta)) = F(W_{dh(d, \vec{s}, \Theta)}, V_{dh(d, \vec{s}, \Theta)}) \\ &= M_{dh(d, \vec{s}, \Theta)}(\Theta) = \max_h \{M_{dh}(\Theta) s_h\}. \end{aligned} \quad (21)$$

In virtue of (19) and (20), we do *not* have to require that there exists a sufficient statistics  $T_1(y) = y$ , so the definition applies for all exponential family distributions. If  $T_1(y) = y$ , we get  $F(w, v) = w$ . Consequently, we drop back to the more trivial case of  $M_{dh}(\Theta) = W_{dh}$ .

The definitions of  $\bar{W}_d(\vec{s}, \Theta)$  and  $\bar{V}_d(\vec{s}, \Theta)$  are relatively technical. However, they define a link  $\vec{\eta}_d(\vec{s}, \Theta)$  for the generative model which is a consistent generalization of the maximum non-linearity (18) used, e.g., for Gaussian observables [32]: Independently of the choice of the observable distribution, the link  $\vec{\eta}_d(\vec{s}, \Theta)$  defined by (19) and (20) ensures that the latents change the means of the observables always according to the maximum superposition model.



The definition of the functions  $\bar{W}_d(\vec{s}, \Theta)$  and  $\bar{V}_d(\vec{s}, \Theta)$  using Eqns. (19) and (20) finalizes the definition of the family of generative models we here consider. The complete model family is defined by (6) to (8) and link (9) with (19) and (20). In analogy to previous models defined using the maximum non-linearity [19], we will refer to family of models as *exponential family MCA* model (ef-MCA). While the ef-MCA data model is very general, we will later see that the chosen parameterization nevertheless results in generic equations for parameter updates. Before, let us consider a canonical example of the family.

**Example 2:** Let us again consider the Gaussian case of Example 1. For the ef-MCA model, the matrix  $M(\Theta)$  is (because of  $T_1(y) = y$ ) given by  $M_{dh}(\Theta) = W_{dh}$  and

$$\bar{W}_d(\vec{s}, \Theta) = W_{dh(d, \vec{s}, \Theta)} = \max_h \{W_{dh} s_h\} \quad (22)$$

$$\bar{V}_d(\vec{s}, \Theta) = V_{dh(d, \vec{s}, \Theta)}.$$

Using (5) with  $\vec{\Phi}$  given by (11), we again obtain  $\vec{\eta}_d(\vec{s}, \Theta)$  as given by (12) but this time with the  $\bar{W}_d(\vec{s}, \Theta)$  and  $\bar{V}_d(\vec{s}, \Theta)$  as in (22). In terms of the normal Gaussian parameterization, we would thus obtain as noise model:

$$p(y_d; \vec{\eta}_d(\vec{s}, \Theta)) = \mathcal{N}(y_d; \bar{W}_d(\vec{s}, \Theta), \bar{V}_d(\vec{s}, \Theta) - \bar{W}_d^2(\vec{s}, \Theta)).$$

The matrix  $V \in \Theta$  thus allows for the latents to also parameterize the variance. We will later see how this parameterization can also be changed back to the normal parameterization using a matrix  $\sigma_{dh}^2 = V_{dh} - W_{dh}^2$  instead of  $V_{dh}$  (which is a more familiar parameterization). Note, however, the transition from a scalar variance (as usually used) to a matrix as variance. Such a generalization, to the best of our knowledge, has not been considered before and the data model presented in (6)-(8) together with (9), (19) and (20) is the first non-linear SC model which allows for the training of two matrices (one corresponding to the mean of observables,  $W$ , and another which parameterizes the variances,  $V$ ). This feature makes the data model more flexible compared to previous approaches (e.g. [32, 25]) and provides more information about the given dataset. The generalized Gaussian model was recently applied to model the statistics of natural image patches [47] where standard Gabor-like generative fields were obtained together with variance profiles per latent variable. The new statistical properties captured by the novel matrices  $V$  can predict richer response properties of simple cells in primary visual cortex (V1) than conventional modelling using one matrix  $W$  for the mean responses. If we wanted to enforce scalar variances (as conventionally used), we could define  $\bar{V}_d(\vec{s}, \Theta)$  as in (13).  $\square$

### 3 Parameter Optimization

Having defined the family of ef-MCA models, we now seek parameters  $\Theta$  that optimize a given model for a given set of data points  $\vec{y}^{(1)}, \dots, \vec{y}^{(N)}$ .

#### 3.1 Maximum Likelihood

We follow a standard maximum likelihood approach and seek parameters  $\Theta$  that optimize the log-likelihood  $\mathcal{L}(\Theta) = \sum_n \log(p(\vec{y}^{(n)} | \Theta))$ . Instead of maximizing the likelihood directly, we optimize a lower bound. For an ef-MCA model the bound is given by:

$$\mathcal{F}(q, \Theta) = \sum_{n, \vec{s}} q^{(n)}(\vec{s}) \{ \sum_d \log(p(y_d^{(n)}; \vec{\eta}_d(\vec{s}, \Theta))) + \sum_h \log(p(s_h | \Theta)) \} + \mathcal{H}(q) \quad (23)$$

where  $\mathcal{H}(q)$  is the Shannon entropy term. The distributions  $q^{(n)}$  can be the exact posteriors  $q^{(n)}(\vec{s}) = p(\vec{s}|\vec{y}^{(n)}, \Theta)$  for tractable models or they can represent variational approximations otherwise. In the latter case, the bound  $\mathcal{F}(q, \Theta)$  is the variational lower bound a.k.a. free energy [48] or ELBO [49]. The lower bound can be optimized iteratively w.r.t. distributions  $q$  (the E-step) and w.r.t. the model parameters  $\Theta$  (the M-step); where the terms ‘E-step’ and ‘M-step’ derive from the optimization steps of the Expectation Maximization algorithm (EM; [50, 48]). The central challenge we have to address for ef-MCA data models is the derivation of parameter update equations which maximize the lower bound.

### 3.2 Parameter Update Equations

Following the standard procedure, we will set the derivatives of  $\mathcal{F}(q, \Theta)$  w.r.t. all model parameters to zero, and derive parameter update rules from the resulting equation system. The derivatives of  $\mathcal{F}(q, \Theta)$  will contain derivatives of  $\bar{W}_d(\vec{s}, \Theta)$  and  $\bar{V}_d(\vec{s}, \Theta)$ . Note that for these derivatives the following applies:

$$\frac{\partial}{\partial W_{dh}} \bar{W}_d(\vec{s}, \Theta) = \mathcal{A}_{dh}(\vec{s}, \Theta), \quad \frac{\partial}{\partial W_{dh}} \bar{V}_d(\vec{s}, \Theta) = 0 \quad (24)$$

$$\frac{\partial}{\partial V_{dh}} \bar{V}_d(\vec{s}, \Theta) = \mathcal{A}_{dh}(\vec{s}, \Theta), \quad \frac{\partial}{\partial V_{dh}} \bar{W}_d(\vec{s}, \Theta) = 0 \quad (25)$$

where

$$\mathcal{A}_{dh}(\vec{s}, \Theta) := \begin{cases} 1 & h = h(d, \vec{s}, \Theta) \\ 0 & \text{otherwise} \end{cases} \quad (26)$$

which follows simply from considering the cases  $h = h(d, \vec{s}, \Theta)$  and  $h \neq h(d, \vec{s}, \Theta)$  separately.

Function  $\mathcal{A}_{dh}(\vec{s}, \Theta)$  has a useful property that we will exploit further below. For special cases of ef-MCA, this property has been observed before [19, 32] but the following Lemma represents the required generalization for exponential family observables:

**Lemma 1** *Consider  $\bar{W}_d(\vec{s}, \Theta)$  and  $\bar{V}_d(\vec{s}, \Theta)$  that are defined in (20). For any well-behaved function  $g(\cdot)$  and any arbitrary  $\vec{s} \in \{0, 1\}^H$ , we have*

$$\mathcal{A}_{dh}(\vec{s}, \Theta)g(\bar{W}_d(\vec{s}, \Theta)) = \mathcal{A}_{dh}(\vec{s}, \Theta)g(W_{dh}) \quad (27)$$

and likewise

$$\mathcal{A}_{dh}(\vec{s}, \Theta)g(\bar{V}_d(\vec{s}, \Theta)) = \mathcal{A}_{dh}(\vec{s}, \Theta)g(V_{dh}). \quad (28)$$

**Proof 1** *For each pair  $(d_o, h_o)$  either of the following applies:*

$$h_o = h(d_o, \vec{s}, \Theta), \quad \text{or} \quad h_o \neq h(d_o, \vec{s}, \Theta).$$

*First, let  $h_o = h(d_o, \vec{s}, \Theta)$ , then it follows from (20)*

$$\mathcal{A}_{d_o h_o}(\vec{s}, \Theta)g(\bar{W}_{d_o}(\vec{s}, \Theta)) = \mathcal{A}_{d_o h_o}(\vec{s}, \Theta)g(W_{d_o h(d_o, \vec{s}, \Theta)}) = \mathcal{A}_{d_o h_o}(\vec{s}, \Theta)g(W_{d_o h_o}).$$

*In the second case, it follows from  $h_o \neq h(d_o, \vec{s}, \Theta)$  and (26) that  $\mathcal{A}_{d_o h_o}(\vec{s}, \Theta) = 0$  which trivially satisfies the claim. The proof of equation (28) is analog.  $\square$*

Having defined the ef-MCA model in Sec.2 and using Lemma 1, we can now prove the main result of this study: we derive concise equations for  $W$  and  $V$  that guarantee that all derivatives of  $\mathcal{F}(q, \Theta)$  w.r.t.  $W_{dh}$  and  $V_{dh}$  vanish. These equations can then be used for parameter updates in an EM algorithm.

**Theorem 1** Consider an ef-MCA data model (6)-(8) with  $p(y; \vec{\eta})$  being an exponential family distribution with  $L = 2$ . Let the parameters  $\Theta$  contain the matrices  $W, V \in \mathbb{R}^{D \times H}$  and let  $\vec{\eta}_d(\vec{s}, \Theta)$  be defined as in Eqns. (9) and (19)-(20). Then the derivatives of the variational lower bound (23) w.r.t. all matrix elements  $W_{dh}$  and  $V_{dh}$  are zero if for all  $d$  and  $h$  applies:

$$W_{dh} = \frac{\sum_{n=1}^N \langle \mathcal{A}_{dh}(\vec{s}, \Theta) \rangle_{q^{(n)}} T_1(y_d^{(n)})}{\sum_{n=1}^N \langle \mathcal{A}_{dh}(\vec{s}, \Theta) \rangle_{q^{(n)}}} \quad (29)$$

and

$$V_{dh} = \frac{\sum_{n=1}^N \langle \mathcal{A}_{dh}(\vec{s}, \Theta) \rangle_{q^{(n)}} T_2(y_d^{(n)})}{\sum_{n=1}^N \langle \mathcal{A}_{dh}(\vec{s}, \Theta) \rangle_{q^{(n)}}} \quad (30)$$

where  $\mathcal{A}_{dh}(\vec{s}, \Theta)$  is given by (26).

**Proof 2** Consider a single dictionary element  $W_{dh}$  and let us abbreviate  $\bar{W}_d = \bar{W}_d(\vec{s}, \Theta)$  and  $\bar{V}_d = \bar{V}_d(\vec{s}, \Theta)$ . Then using the chain rule, we obtain

$$\begin{aligned} \frac{\partial}{\partial W_{dh}} \log(p(y_d; \vec{\eta}_d(\vec{s}, \Theta))) &= \frac{\partial}{\partial W_{dh}} \log(p(y_d; \vec{\Phi}(\bar{W}_d, \bar{V}_d))) \\ &= \sum_{l=1}^2 \left( \frac{\partial}{\partial W_{dh}} \Phi_l(\bar{W}_d, \bar{V}_d) \right) \left( \frac{\partial}{\partial \eta_l} \log(p(y_d; \vec{\eta})) \Big|_{\vec{\eta}=\vec{\Phi}(\bar{W}_d, \bar{V}_d)} \right) \\ &= \sum_{l=1}^2 \left( \frac{\partial}{\partial W_{dh}} \bar{W}_d \right) \left( \frac{\partial}{\partial w} \Phi_l(w, \bar{V}_d) \Big|_{w=\bar{W}_d} \right) \left( \frac{\partial}{\partial \eta_l} \log(p(y_d; \vec{\eta})) \Big|_{\vec{\eta}=\vec{\Phi}(\bar{W}_d, \bar{V}_d)} \right) \\ &= \sum_{l=1}^2 \left( \mathcal{A}_{dh}(\vec{s}, \Theta) \right) \left( \frac{\partial}{\partial w} \Phi_l(w, \bar{V}_d) \Big|_{w=\bar{W}_d} \right) \left( T_l(y_d^{(n)}) - \frac{\partial A(\vec{\eta})}{\partial \eta_l} \Big|_{\vec{\eta}=\vec{\Phi}(\bar{W}_d, \bar{V}_d)} \right). \end{aligned} \quad (31)$$

Moreover, we know that for a distribution of the exponential family,  $A(\vec{\eta})$  satisfies (see [41] for more information):

$$\frac{\partial A(\vec{\eta})}{\partial \eta_1} = \langle T_1(y) \rangle_{p(y; \vec{\eta})} \quad \text{and} \quad \frac{\partial A(\vec{\eta})}{\partial \eta_2} = \langle T_2(y) \rangle_{p(y; \vec{\eta})} \quad (32)$$

for finite  $A(\eta)$ . Thus, we can further simplify:

$$\begin{aligned}
\frac{\partial}{\partial W_{dh}} \log(p(y_d; \vec{\eta}_d(\vec{s}, \Theta))) &= \sum_{l=1}^2 \left( \mathcal{A}_{dh}(\vec{s}, \Theta) \right) \left( \frac{\partial}{\partial w} \Phi_l(w, \bar{V}_d) \Big|_{w=\bar{W}_d} \right) \\
&\times \left( T_l(y_d^{(n)}) - \langle T_l(y) \rangle_{p(y; \vec{\eta})} \right) \Big|_{\vec{\eta}=\vec{\Phi}(\bar{W}_d, \bar{V}_d)} \\
&= \sum_{l=1}^2 \left( \mathcal{A}_{dh}(\vec{s}, \Theta) \right) \left( \frac{\partial}{\partial w} \Phi_l(w, \bar{V}_d) \Big|_{w=\bar{W}_d} \right) \left( T_l(y_d^{(n)}) - \langle T_l(y) \rangle_{p(y; \vec{\Phi}(\bar{W}_d, \bar{V}_d))} \right).
\end{aligned} \tag{33}$$

Now, using Lemma 1 we obtain

$$\begin{aligned}
\frac{\partial}{\partial W_{dh}} \log(p(y_d; \vec{\eta}_d(\vec{s}, \Theta))) &= \sum_{l=1}^2 \left( \mathcal{A}_{dh}(\vec{s}, \Theta) \right) \left( \frac{\partial}{\partial w} \Phi_l(w, V_{dh}) \Big|_{w=W_{dh}} \right) \\
&\times \left( T_l(y_d^{(n)}) - \langle T_l(y) \rangle_{p(y; \vec{\Phi}(W_{dh}, V_{dh}))} \right).
\end{aligned} \tag{34}$$

Note that the above equation depends on parameter  $\vec{s}$  of the hidden states only through function  $\mathcal{A}_{dh}(\vec{s}, \Theta)$ . This is an important property of the Lemma 1 that alleviates the complexity of the aforementioned equations and enables us to provide simple update equations for the dictionaries  $W$  and  $V$  of the model. To see this, we derive:

$$\begin{aligned}
\frac{\partial}{\partial W_{dh}} \mathcal{F}(q, \Theta) &= \sum_n \sum_{\vec{s}} q^{(n)}(\vec{s}) \frac{\partial}{\partial W_{dh}} \log(p(y_d^{(n)}; \vec{\eta}_d(\vec{s}, \Theta))) \\
&= \sum_n \sum_{\vec{s}} q^{(n)}(\vec{s}) \sum_{l=1}^2 \left( \mathcal{A}_{dh}(\vec{s}, \Theta) \right) \left( \frac{\partial}{\partial w} \Phi_l(w, V_{dh}) \Big|_{w=W_{dh}} \right) \\
&\times \left( T_l(y_d^{(n)}) - \langle T_l(y) \rangle_{p(y; \vec{\Phi}(W_{dh}, V_{dh}))} \right) \\
&= \sum_{l=1}^2 \left( \frac{\partial}{\partial w} \Phi_l(w, V_{dh}) \Big|_{w=W_{dh}} \right) \sum_n \langle \mathcal{A}_{dh} \rangle_{q^{(n)}} \\
&\times \left( T_l(y_d^{(n)}) - \langle T_l(y) \rangle_{p(y; \vec{\Phi}(W_{dh}, V_{dh}))} \right) \\
&= \left( \frac{\partial}{\partial w} \Phi_1(w, V_{dh}) \Big|_{w=W_{dh}} \right) \sum_n \langle \mathcal{A}_{dh} \rangle_{q^{(n)}} \left( T_1(y_d^{(n)}) - W_{dh} \right) \\
&+ \left( \frac{\partial}{\partial w} \Phi_2(w, V_{dh}) \Big|_{w=W_{dh}} \right) \sum_n \langle \mathcal{A}_{dh} \rangle_{q^{(n)}} \left( T_2(y_d^{(n)}) - V_{dh} \right)
\end{aligned} \tag{35}$$

where in the last equation we exploited our mean value parameterization defined as  $\vec{w} := \langle \vec{T}(y) \rangle_{p(y; \vec{\Phi}(\vec{w}))}$ . Now, independently of the functions  $\frac{\partial}{\partial w} \Phi_l(w, V_{dh}) \Big|_{w=W_{dh}}$ , the derivative of the

lower bound w.r.t.  $W_{dh}$  is zero, i.e.  $\frac{\partial \mathcal{F}}{\partial W_{dh}} = 0$ , if we set

$$\sum_n \langle \mathcal{A}_{dh}(\vec{s}, \Theta) \rangle_{q^{(n)}} (T_1(y_d^{(n)}) - W_{dh}) = 0 \quad (36)$$

and

$$\sum_n \langle \mathcal{A}_{dh}(\vec{s}, \Theta) \rangle_{q^{(n)}} (T_2(y_d^{(n)}) - V_{dh}) = 0. \quad (37)$$

Rearranging terms yields equations (29) and (30) which completes the proof. The proof proceeds along the same lines for  $\frac{\partial \mathcal{F}}{\partial V_{dh}}$ .  $\square$

Fulfilling equations (29) and (30) guarantees vanishing derivatives, and in practice the equations can be used to increase the variational lower bound to (possibly local) maxima. We do remark, however, that we have not strictly proven that equations (29) and (30) correspond to a maxima (and not minima or saddle points). In addition, observe that a straightforward outcome of the foregoing theorem is when the distribution does contain a sufficient statistics proportional to  $y$ , i.e.  $T_1(y) = y$ , that yields a further simplification of the algorithm:

**Corollary 1** *Prerequisites as for Theorem 1. If the distribution  $p(y; \vec{\eta})$  has sufficient statistics  $T_1(y) = y$ , then the condition for  $W_{dh}$  is given by:*

$$W_{dh} = \frac{\sum_{n=1}^N \langle \mathcal{A}_{dh}(\vec{s}, \Theta) \rangle_{q^{(n)}} y_d^{(n)}}{\sum_{n=1}^N \langle \mathcal{A}_{dh}(\vec{s}, \Theta) \rangle_{q^{(n)}}}. \quad (38)$$

The corollary finally explains why the update equation for the original MCA data model [19] (which used Poisson noise) and the update equation for later MCA models [32, 17, 20] (which used Gaussian noise) are identical and given by (38).

Finally observe that the equations (29) and (30) do not represent closed-form solutions for  $W$  and  $V$  because the right-hand-sides also depend on  $W$  and  $V$  through the function  $\mathcal{A}_{dh}(\vec{s}, \Theta)$ . Following previous work [19, 32], we can, however, use equations (29) and (30) in the fixed-point sense, i.e., we update:

$$W_{dh}^{\text{new}} = \frac{\sum_{n=1}^N \langle \mathcal{A}_{dh}(\vec{s}, \Theta^{\text{old}}) \rangle_{q^{(n)}} T_1(y_d^{(n)})}{\sum_{n=1}^N \langle \mathcal{A}_{dh}(\vec{s}, \Theta^{\text{old}}) \rangle_{q^{(n)}}} \quad (39)$$

and

$$V_{dh}^{\text{new}} = \frac{\sum_{n=1}^N \langle \mathcal{A}_{dh}(\vec{s}, \Theta^{\text{old}}) \rangle_{q^{(n)}} T_2(y_d^{(n)})}{\sum_{n=1}^N \langle \mathcal{A}_{dh}(\vec{s}, \Theta^{\text{old}}) \rangle_{q^{(n)}}} \quad (40)$$

where also  $q^{(n)} = q^{(n)}(\vec{s}; \Theta^{\text{old}})$  depends on the old parameters. If repeated updates result in the values of  $W$  and  $V$  to converge, then the converged values fulfill Eqns. (29) and (30), respectively.

To complete the parameter updates, we can also derive updates for the prior parameters  $\vec{\pi}$ . Those derivations do not involve the specific form of the observables' distribution. We can therefore use previous derivations [8, 25] and update  $\vec{\pi}$  as follows:

$$\pi_h^{\text{new}} = \frac{1}{N} \sum_{n=1}^N \langle s_h \rangle_{q^{(n)}}, \quad h = 1, \dots, H. \quad (41)$$

We derived Theorem 1 for the case of  $L = 2$ , i.e., for two-parameter distributions of the exponential family. This choice was for notational convenience only. Considering the proof of Theorem 1, it can be observed that it relatively directly generalizes to any number of  $L$ . We provide the general proof in the Appendix A.

### 3.3 EM Algorithm for ef-MCA

The main focus of the previous section was the derivation of the parameter update equations (the M-step). Regarding the E-step, exact posteriors, i.e.  $q^{(n)}(\vec{s}) = p(\vec{s} | \vec{y}^{(n)}, \Theta)$ , can be computed for small scale ef-MCA models where the parameters will be updated according to Eqns. (39)-(41). For larger scale problems, we require approximations for optimization. In our experiments below, we thus use a recent variational approximation (variational E-step) which is applicable to any observable distribution of the exponential family (see [51]). The approach uses truncated posteriors as approximation which are of the form:

$$q^{(n)}(\vec{s} | \vec{y}^{(n)}, \Theta, \mathcal{K}^{(n)}) := \frac{p(\vec{s} | \vec{y}^{(n)}, \Theta)}{\sum_{\vec{s}' \in \mathcal{K}^{(n)}} p(\vec{s}' | \vec{y}^{(n)}, \Theta)} \delta(\vec{s} \in \mathcal{K}^{(n)}). \quad (42)$$

Distributions (42) approximate full posteriors by truncating sums over the whole latent space to sums over those subsets  $\mathcal{K}^{(n)}$  which accumulate most of the posterior mass [52, 51]. The subsets  $\mathcal{K}^{(n)}$  can then be updated, e.g., using evolutionary algorithms with fitness defined to be a monotonic function of the model joint  $p(\vec{s}, \vec{y} | \Theta)$ . The method does not require derivations, and is thus applicable ‘black box’ to any distribution of the exponential family.

The concrete EM algorithm for training the proposed data model is then given by Alg. 1 for a two-parameter distribution ( $L = 2$ ). Note that for one-parameter distributions ( $L = 1$ ), dependencies are just on  $\bar{W}$ .

## 4 Numerical Verification and Example Applications

We now numerically verify the derived update equations using different well-known distributions of the exponential family as examples. Concretely, we use Bernoulli, Poisson, Exponential, Gaussian and the Gamma distributions and optimize the corresponding ef-MCA models with EM presented by Alg. 1. We use the result of Theorem 1 for the M-steps while for the E-steps, we use the full posteriors when the used models are sufficiently small and apply approximations (42) otherwise. For technical details of the experiments we refer to Appendix B.

### 4.1 Artificial Data

We first use a standard artificial data set, the bars test [53, 19], to verify and evaluate the derived update equations. We are particularly interested in how well the updates can recover the true generating parameters. For data generated by the corresponding data model itself, parameters should (for sufficiently many data points and modulo symmetries) be recovered with very high

---

**Algorithm 1:** Exact EM algorithm for parameter updates

---

initialize model parameters  $\Theta = (\vec{\pi}, W, V)$ ;

**repeat**

    compute the inverse mapping  $\vec{\Phi}$  defined in (5);

**if** the distribution  $p(y; \vec{\eta})$  has sufficient statistics  $T_1(y) = y$  **then**

$M(\Theta) = W$ ;

**else**

        compute the function  $F$  in (19) based on the relation of the natural parameters  $\vec{\eta}$  and the first moment of  $p(y; \vec{\eta})$ ;

$M(\Theta) = F(W, V)$ ;

**end**

**for** each vector  $\vec{s}$  of the latent space **do**

**for**  $d = 1 : D$  **do**

$h(d, \vec{s}, \Theta) = \operatorname{argmax}_h \{M_{dh}(\Theta)s_h\}$ ;

$\bar{W}_d = W_{dh(d, \vec{s}, \Theta)}$  and  $\bar{V}_d = V_{dh(d, \vec{s}, \Theta)}$ ;

$\vec{\eta}_d = \vec{\Phi}(\bar{W}_d, \bar{V}_d)$ ;

**end**

**for**  $n = 1 : N$  **do**

$q^{(n)}(\vec{s}) = p(\vec{s} | \vec{y}^{(n)}, \Theta)$ ;

**for**  $h = 1 : H$  and  $d = 1 : D$  **do**

                compute  $\langle s_h \rangle_{q^{(n)}}$ ;

                compute  $\langle \mathcal{A}_{dh} \rangle_{q^{(n)}}$  where  $\mathcal{A}_{dh}$  is defined in (26);

**end**

**end**

**end**

    update parameters  $\Theta$  using Eqns. (39)-(41);

**until** parameters  $\Theta$  have sufficiently converged;

---

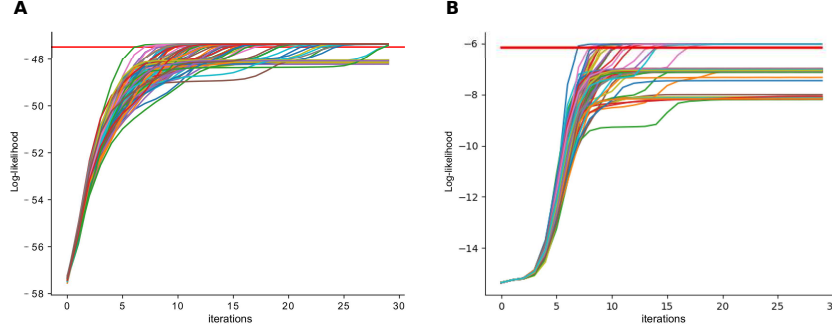


Figure 3: Behaviour of the log-likelihood function corresponding to the (A) E-MCA and (B) B-MCA models for 100 runs using artificial bars test. Different colors denote different runs of the algorithms.

accuracy. Here, we consider Exponential and Bernoulli as one-parameter distributions of the exponential family to assess the efficacy of the results of Theorem 1 in increasing the likelihood of the data using Exponential-MCA (E-MCA) and Bernoulli-MCA (B-MCA) models.

In detail, we used  $H = 10$  basis functions  $\vec{W}_h$  in the form of horizontal and vertical bars each occupying 5 pixels on a  $D = 5 \times 5$  grid. The latents are sampled independently (according to the prior) with probability  $\pi_h$  for  $h = 1, \dots, H$ , and the corresponding generative fields are superimposed non-linearly according to the max function defined in (20). We generated two sets of datapoints using the ef-MCA model: One with Exponential distribution as the observation noise and another with Bernoulli distribution. The corresponding ef-MCA models are then optimized for each of the generated datasets: E-MCA is trained on the generated data with Exponential noise and likewise B-MCA on the data with Bernoulli noise. We stress again that no derivations are required: We only require the evaluation of joint probabilities which are directly given by the prior and the used noise model (here Exponential or Bernoulli distribution). Model parameters  $W$  and  $\vec{\pi}$  were randomly initialized (see Appendix B.1 for details). We repeated this procedure 100 times and closely examined the behaviour of the log-likelihood function for each of the runs. The results are then depicted in Fig. 3.

As can be observed, the update equations of Theorem 1 give rise to a robust and reliable algorithm that monotonically increases the log-likelihood of the data to at least a local log-likelihood optimum (note that we used full posteriors here). The Fig. 3 further illustrates that the algorithm converges to the ground-truth log-likelihood values (red line in Fig. 3) in many runs. In these runs, the learned parameters are very close to the generating ones (with small differences due to finite sample size effects). Nevertheless, local optima can be observed for some cases where the learned log-likelihood values differ from the ground-truth values (see Appendix B.2 for more details). Moreover, Fig. 4 displays the model parameters learned in one such run for the E-MCA algorithm. In general, we also found the sparsity level (the value of  $\vec{\pi}$ ) to be an important factor influencing the outcome of the algorithm in reaching the global optimum: The *reliability* of the algorithm (the probability of recovering all model parameters; compare, e.g., [54, 19]) shows to decrease as the sparsity decreases (increasing number of active hidden units; we elaborate in Appendix B.3).

## 4.2 More Realistic Data

After the initial verification above, let us now point to some example applications on real data. Applications often require large models such that computing full posteriors becomes infeasible.



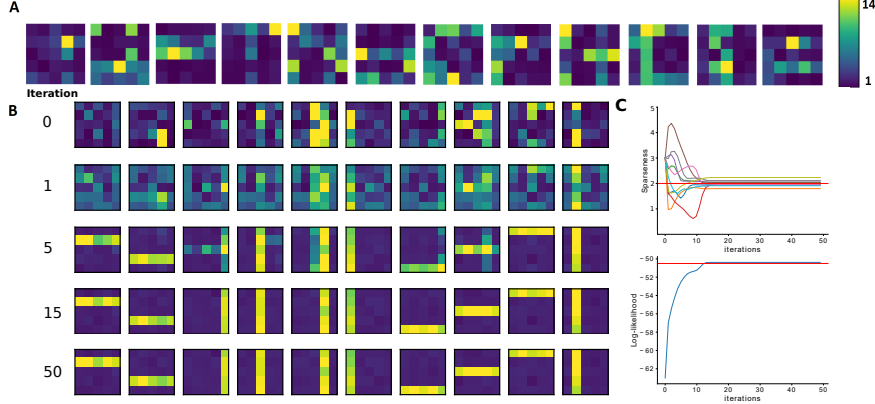


Figure 4: **A** 12 examples of input data. **B** Learned generative fields using E-MCA model where the number of iterations illustrated on the left hand side. **C** Behaviour of the lower bound (bottom) and sparseness ( $\pi_h H$ ; top) for  $h = 1, \dots, H$ . The generating parameter is  $\pi_h H = 2$  for all  $h$ . See Appendix B.1 for details.

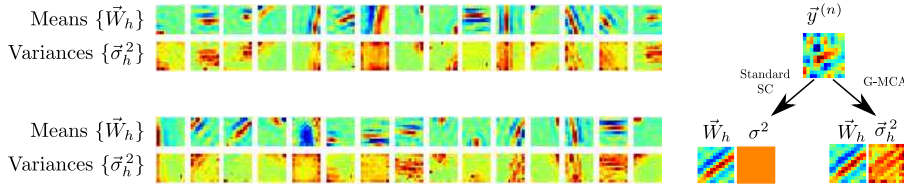


Figure 5: Dictionaries ( $W_{dh}$ ) and ( $\sigma_{dh}^2$ ) learned by G-MCA on natural image patches (30 generative fields each). We show ( $\sigma_{dh}^2$ ) instead of ( $V_{dh}$ ) for better interpretability. The right sketch illustrates the difference between using a standard SC model (scalar  $\sigma^2$ ) and G-MCA. See Appendix B.4 for full dictionaries.

To scale algorithms to larger sizes, we apply variational approximations in the form of truncated posteriors given by (42). Truncated posteriors have previously been used for MCA models with Gaussian noise [32, 55]. Here we use the above mentioned and more recent ‘black box’ variant [51].

**Natural Image Patches.** As the first application to natural data, let us use the model of Example 2 (Sec. 2), i.e., Gaussian-MCA (G-MCA). As discussed previously, the G-MCA model has two matrices that we can optimize using Theorem 1, one for the mean  $W$  and a combination of  $V$  and  $W$  for the variance of the Gaussian. To facilitate interpretation, one can reparameterize the matrices back to the normal Gaussian parameters by setting  $\sigma_{dh}^2 = V_{dh} - W_{dh}^2$  (see Appendix A.2 for details). We trained a G-MCA model on a set of  $N = 100,000$  ZCA-whitened image patches [56]. To the set of patches of size  $D = 12 \times 12$  we applied a model with  $H = 1,000$  components and learned individual dictionaries for component means ( $W_{dh}$ ) and variances ( $\sigma_{dh}^2$ ). In addition, as the considered data encompasses both positive and negative values, we follow [17] and use a maximum magnitude function  $h(d, \vec{s}, \Theta) = \arg\max_h |W_{dh} s_h|$  in (20) (note that  $M(\Theta) = W$  for the case of Gaussian). After learning, we observed a large variety of generative fields (GFs) for the component means (including the familiar Gabor-like and globular fields) as well as a large variety of GFs for component variances. Fig. 5 illustrates 30 examples of such GFs where the full dictionaries are provided in Appendix B.4. The observed variety of variance GFs stands

Table 1: Results of the noise type estimation experiment with noisy ‘house’ images (see text for details). Listed are highest free energies per data point of five runs.

model	Gaussian-MCA	Gamma-MCA
Gaussian-noise	<b>-741.18</b>	-755.12
Gamma-noise	-742.90	<b>-737.00</b>

in contrast to a uniform variance with equal value for all latents as assumed by standard SC or previous MCA versions. Compared to such previous approaches, a generalized encoding of component means alongside of component variances may allow to describe more accurately how first and second order statistics are combined in real world datasets and may be more closely aligned with neural responses in V1 (also see [47]).

As final remark for this experiment, note that it serves to illustrate scalability: Using the above described approximation (42), models with high-dimensional latent spaces (here we used  $H = 1,000$ ) can be trained.

**Noise Type Estimation.** As another example application, we consider the problem of determining the unknown noise type in a given dataset. This problem is of importance for data analysis in a number of applications and is actively researched (see, e.g., [57, 58, 59]; also see Appendix B.5 for a discussion of related work). The result of Theorem 1 does allow for developing approaches to determine the type of the data distribution. As a proof of concept in this direction, we show how, e.g., Gaussian- and Gamma-MCA models can be used to determine which of the two noise distributions is better suited for a given data set.

We here consider the standard ‘house’ image (Fig. 6), to which we either add Gaussian or Gamma noise. We then apply Gaussian- and Gamma-MCA and compare their variational lower bounds (as approximations of their log-likelihoods) on the different data sets. We use a common scenario for both noise models and add Gamma or Gaussian noises with random variance values. Detailed information regarding the variance update of Gaussian-MCA is presented in Examples 1 and 2 and we further discuss it in Appendix A.2. Also the update equation for variance of the Gamma-MCA is presented in Appendix A.3 (note that similar to the Gaussian-MCA model, we use a combination of  $W$  and  $V$  to estimate the variances of the Gamma distributions).

From Tab. 1 we observed that the lower bound of the Gaussian-MCA is higher for the data with Gaussian noise than the lower bound of the Gamma-MCA and vice versa. Although this may be seen as a proof-of-concept example, the experiment reveals that the lower bound comparison can be exploited in a straight-forward manner to distinguish between the two noise types in a given dataset. Here, since we apply the models with the same number of model parameters, we can directly use the lower bounds (as approximate log-likelihoods) for model selection, i.e., we do not have to consider penalty terms for the number of parameters (compare, e.g., AIC or BIC criteria [60]). This example further shows that the updates (39) and (40) can supply sufficiently flexible and precise algorithms for noise estimation also at large scales. Model selection using further types of noise distributions can proceed along the same lines but require a more elaborate treatment (also compare, e.g., [58]) which exceeds the purposes of this study.

**Denoising.** Finally, we use the presented updates to denoise images corrupted by non-Gaussian noise. This task can be considered more difficult compared to the removal of additive white Gaussian noise which numerous established denoising algorithms are optimized for (compare, e.g., [61, 62, 63, 64, 65, 66, 67, 68]). We investigate two different noise types, namely Poisson and Exponential. As datasets, we use the standard benchmark images ‘house’, ‘cameraman’ and ‘pep-

pers’ [61, 27]. From each image we then generate one with added Poisson noise and one with added Exponential noise. As next step, we then apply Poisson-MCA (P-MCA) to denoise the images with Poisson noise and analogously Exponential-MCA (E-MCA) to denoise the images corrupted by Exponential noise. In particular, we consider the non-linear inverse problem (compare [69]) of estimating the non-noisy image only from observing a noisy version of the clean image: P-MCA and E-MCA are directly applied to the noisy image itself without leveraging external, clean training data (this is sometimes also referred to as ‘zero-shot’ learning; compare, e.g., [70, 71]). Mathematically speaking, given a set  $Y_{\text{corrupted}} = F(Y_{\text{original}})$  of corrupted data points ( $F$  denotes a noise operator, in this case Poisson or Exponential), we aim to compute an estimation  $Y_{\text{estimate}}$  of the uncorrupted data  $Y_{\text{original}}$ . As for both Poisson and Exponential distributions the sufficient statistics are  $T(y) = y$  (i.e.,  $M(\Theta) = W$ ), we can follow [51] and use the following estimator<sup>2</sup> for the non-noisy image pixels:

$$(\vec{y}_{\text{estimate}}^{(n)})_d = \langle \bar{W}_d(\vec{s}, \Theta) \rangle_{q^{(n)}}. \quad (43)$$

The family of ef-MCA models allows for treating a much larger variety of noise distributions, of course, but focusing on P- and E-MCA may illustrate the potential also for other noise types which may be encountered in data.

After Gaussian denoising, Poisson noise removal benchmarks do presumably provide the most extensive opportunities for quantitative comparisons of different denoising algorithms. One possibility for denoising an image corrupted with Poisson noise is to simply ignore the specific properties of Poisson noise and employ a method that is tailored to Gaussian noise. For instance, the sparse 3D transform-domain collaborative filtering (BM3D) [72] can be applied directly. BM3D is a well-known denoising method which often outperforms sparse coding or k-SVD [73] algorithms on image denoising benchmarks. The method is tailored to 2D-images corrupted by Gaussian noise but, as mentioned, can also be applied to Poisson noise removal to certain extents.

A frequently followed alternative approach is to first convert Poisson noise into Gaussian noise, and then apply an algorithm which assumes Gaussian observables. Such methods apply a non-linear variance stabilization transform (VST) such as Anscombe [74] and Fisz [75] that produces a signal in which the noise can approximately be treated as additive Gaussian with unit variance. Approaches such as VST+BM3D use the Anscombe root transformation followed by standard BM3D in this case (see, e.g. [76]; we also elaborate further in Appendix B.6). Such transformation-based approaches are specific to the Poisson noise as similar transformations are not in general available for exponential family distributions. But also in the case of Poisson noise, transformation to Gaussian noise can be problematic. In fact, it is known that transformation-based methods can yield poor results for low-intensity signals (see [27, 76]). It should be noted that the Poisson noise is not additive and the image intensity (or the peak value of the original image) determines the strength of the noise (the lower the peak, the stronger the noise). For low peak values (e.g. lower than 3), VST transformations are less effective. As a result, many approaches have been suggested to improve such transformations or exploit alternative approaches that yield better results in the case of low-intensity signals [27, 76, 77, 78, 44, 79]. One example is the P<sup>4</sup>IP approach [77] that applies a general plug-and-play-prior approach on Poisson inverse-problems. The method still relies on Gaussian-based denoising algorithms, however. Other studies (e.g. [76, 78]) attempt to improve the transformation techniques and therefore increase the performance of the methods. For instance, an iterative VST framework (known as I+VST+BM3D) is established by Azzari and Foi [78] that can cope with extreme low signal-to-noise ratio (SNR) cases.

More relevant for comparison to our approach are methods that explicitly assume a Poisson noise.

---

<sup>2</sup>Estimators of other distributions would use the corresponding  $M(\Theta)$  matrix.

Table 2: PSNR comparison for the considered Poisson denoising benchmarks. PSNR values are shown in terms of dB; values of BM3D, VST+BM3D, I+VST+BM3D, P<sup>4</sup>IP, DenoiseNet, NLSPCA and SPDA are taken from [78, 76, 80]. The considered algorithms are divided into two groups. BM3D, VST+BM3D, I+VST+BM3D and P<sup>4</sup>IP are highly engineered algorithms that assume a Gaussian noise model. Also DenoiseNet is a deep learning-based algorithm that uses a large number of training data. NLSPCA, SPDA and P-MCA, on the other hand, are based on the assumption of a Poisson noise model (see text for more information). The bold number in each subgroup denotes the best PSNR value in comparison to the other models of the subgroup; the bold and underlined number denotes the best PSNR value amongst all the models. As illustrated, P-MCA represents a competitive performance compared to BM3D, VST+BM3D, I+VST+BM3D and P<sup>4</sup>IP, and outperforms NLSPCA and SPDA in 5 out of 6 cases that are considered here. \*This is the value reported by the P<sup>4</sup>IP authors in their arXiv paper [77], and this value is also used by other later contributions for comparison (e.g. [78, 80]); but we remark that another value (22.33, i.e., the second digit is different) is reported in the journal version.

Method	Peak	House	Cameraman	Peppers
BM3D	2	24.18	22.13	21.97
VST+BM3D		23.79	21.97	22.02
I+VST+BM3D		24.62	22.25	21.93
P <sup>4</sup> IP		24.65	21.87	21.33*
DenoiseNet		<b><u>24.77</u></b>	<b><u>23.25</u></b>	<b><u>23.19</u></b>
NLSPCA		23.16	20.64	20.48
SPDA		<b>24.37</b>	21.35	21.18
P-MCA		23.51	<b>21.79</b>	<b>22.03</b>
BM3D	4	26.04	23.94	24.07
VST+BM3D		25.49	23.82	24.01
I+VST+BM3D		26.07	24.10	24.04
P <sup>4</sup> IP		26.33	23.29	23.88
DenoiseNet		<b><u>26.59</u></b>	<b><u>24.87</u></b>	<b><u>24.83</u></b>
NLSPCA		24.26	20.97	21.07
SPDA		25.30	21.72	22.20
P-MCA		<b>26.14</b>	<b>23.42</b>	<b>23.87</b>

One important study is the work by Salmon et al. [27, NLSPCA] that uses Poisson PCA in which the link between latents and observables (as discussed in the introduction) is considered to be a weighted linear sum that sets the Poisson’s natural parameter. In another study, Giryes and Elad [44, SPDA] introduce a Poisson sparse model capable of learning dictionaries from a Poisson distributed dataset. Their method likewise considers a linear superposition of the latents. Despite these two approaches, the P-MCA model we use here exploits a non-linear (maximum) superposition of the latents that sets the mean of observables. Moreover, this model is only one example of the general result represented by Theorem 1.

In addition to the approaches presented above, deep learning-based techniques have also been applied to Poisson denoising in recent years (see, e.g., [80, 81, 82, 83, 84]). Importantly, Remez et al. [80, DenoiseNet] explore deep convolutional neural networks (CNNs) to denoise low-light images. The proposed DenoiseNet has shown to establish state-of-the-art results for Poisson denoising. Nonetheless, there are substantial differences between, for instance, DenoiseNet and P-MCA: P-MCA is trained directly on the noisy image and the approach does not require a-priori information about the peak value of the corrupted data; this contrasts with DenoiseNet which

requires external training data and which is optimized for a specific peak value. In another recently published work [81], authors use multi-directional long-short term memory (LSTM) networks along with the CNNs that can also capture and learn the statistics of residual noise components. The method can further achieve better results in comparison to the DenoiseNet. Describing all the details of the aforementioned studies, however, is far from our goals here and we refer the readers to the corresponding papers for details.

Tab. 2 presents a quantitative performance comparison of the different approaches using the standard measure of peak-signal-to-noise-ratio (PSNRs). The methods we chose for comparison in Tab. 2 represent, to our best knowledge, the state-of-the-art results of Poisson denoising for different peak values. As can be observed, P-MCA produces competitive results but can be outperformed by BM3D, VST+BM3D, I+VST+BM3D, P<sup>4</sup>IP or DenoiseNet. At closer inspection, these five approaches are all using considerable fine-tuning specific to images. Also the first four algorithms are based on a Gaussian assumption (potentially after preprocessing). P-MCA is like SPDA and NLSPCA not tailored to images. All these three approaches also have in common that they are directly based on the assumption of a Poisson distribution for the observables. While both NLSPCA and SPDA assume a linear superposition link to the natural parameters, P-MCA assumes a maximum superposition for the Poisson mean. Considering Tab. 2, P-MCA shows in comparison to SPDA and NLSPCA improved performance in terms of PSNR values in five out of the six investigated settings. Such improvements for one example of the exponential family (P-MCA) may argue in favor of the general approach represented by the proposed latent variable model and its optimization based on Theorem 1. Furthermore, even compared to approaches such as BM3D, VST+BM3D, I+VST+BM3D, P<sup>4</sup>IP or DenoiseNet, which are image specific and highly optimized for denoising tasks, P-MCA shows comparable results. Fig. 6 further illustrates the reconstructed house, cameraman and peppers images using the P-MCA model. The estimated house image can be further compared with Fig. 9 depicted in [44] which presents the results of BM3D, SPDA and NLSPCA methods.

For Exponential noise (E-MCA), a similar comparison as for the Poisson noise is not possible because, to the best of our knowledge, no other latent variable model is tailored to the removal of exponential noise. Consequently, E-MCA illustrates an example where the general result of Theorem 1 gives rise to an algorithm directly applicable to less commonly encountered noise types (such as Exponential). Fig. 7 illustrates the results for denoising an image with exponential noise. We here compare the performance of the E-MCA with other MCA models, P-MCA and G-MCA (Gaussian-MCA), and BM3D, VST+BM3D and spike-and-slab sparse coding (SSSC) [12, 85]. The SSSC is also a sparse coding approach with a flexible prior distribution that assumes a Gaussian noise model. As can be observed from Fig. 7, E-MCA achieves the highest PSNR value compared to all other approaches. This result might be considered intuitive as the Exponential noise model of E-MCA is most closely aligned with the Exponential noise distribution of the noisy image. In addition, P- and G-MCA models perform reasonably well in comparison to SSSC; and VST+BM3D is shown to perform the worst, which can be attributed to the VST transformation being specific to Poisson noise.

Consistent with the higher PSNRs, we observe that, e.g., P-MCA better recovers the structure of the original image when the noise is Poisson and vice versa for E-MCA. This, however expected, further highlights the importance of tasks such as noise type estimation and model selection. Further, the results emphasize the utility and practical applicability of the presented approach for optimization of non-linear generative models. Visual inspection may even argue in favor of using the right noise model more than what PSNR values would suggest. Fig. 7 shows, for instance, larger differences between E-MCA compared to BM3D than may be expected by considering the PSNR values of the two approaches.



(a) Original image      (b) Corrupted image      (c) Denoised with P-MCA

Figure 6: Denoising of the house, cameraman and peppers images when corrupted with Poisson noise (the peak values of the house and peppers images are 2 and of the cameraman is 4). The figure illustrates the original and noisy images together with the reconstructed images using P-MCA. The corresponding PSNR values are further presented in Tab. 2. In addition, the denoised house image can be compared with Fig. 9 of [44] which depicts the reconstructed images using BM3D, SPDA and NLSPCA methods.

## 5 Discussion

Latent variable models have found very wide-spread use in Machine Learning, Statistics and Artificial Intelligence applications. A central element of all these algorithms is the update equation for the matrices that couple latent variables to observables (the dictionaries). Maybe most prominently, the specific form of dictionary updates suggested for non-negative matrix factorization (NMF) is a hallmark of one of the seminal papers for dictionary learning [86]. For any model with a non-linear superposition of generative fields, the derivation of dictionary updates is a challenge because closed-form solutions are typically not obtainable [36, 87, 19, 35, 37]. For many types of data, a non-linear superposition can, however, be more closely aligned with the true data generating process (see [18, 19, 17, 88, 20] for more discussions). If an algorithm aims to find a dictionary containing the true structural primitives for such data, then update rules derived from the corresponding non-linearities are required.

A non-linearity which may be considered as a natural alternative to summation of latents is maximization. The maximum has been investigated for occlusion like non-linearities in image data [19, 32, 17] as well as for masking based non-linearities in sounds [18, 19, 20]. While it would be challenging to address the maximum non-linearity with any gradient based approaches, it has

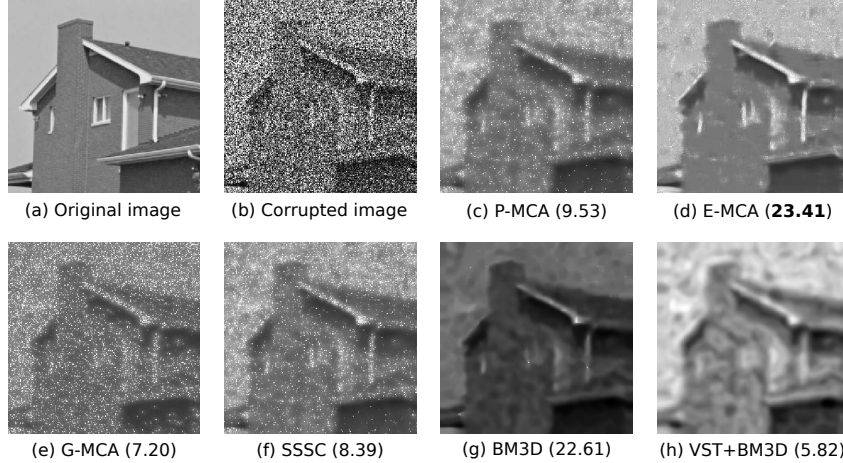


Figure 7: Denoising of the house image when heavily corrupted with Exponential noise (peak = 255). Depicted are reconstructed images and corresponding PSNR values in dB obtained with different models (see text for details). Here, E-MCA achieves the highest PSNR value in comparison to the others which is consistent with the Exponential noise. Also note that P- and E-MCA use one-parameter distributions as noise models and only use the information of one dictionary (related to the mean of the distribution); whilst the other models (G-MCA, SSSC and BM3D) use additional parameters to additionally model second-order statistics.

convenient analytical properties which can be exploited. These properties allowed us here to derive our main result: A general set of parameter update equations applicable to any distribution of the exponential family. The maybe most closely related approach, exponential family SC (EF-SC) [31], used MAP-based optimization and distributions of the exponential family with a linear superposition which defined the natural parameters of the used observation noise. Such a link from latents to observables has advantages in terms of MAP-based training (monomodal posteriors are maintained). A disadvantage is that different observable distributions essentially define different non-linear superposition models (because the natural parameters are in general non-linear functions of the mean). Also how a coupling to two (or more) parameter distributions can be realized seems to be an open question for previous approaches. At least, neither EF-SC nor PCA-like approaches which use the same coupling [28, 29, 27] report numerical results for more than one-parameter distributions of the exponential family. Additionally, EF-SC would not be able to learn prior parameters because of the used MAP approaches (additional cross-validation would be required). In contrast, the model presented here is generally defined with parameter update equations (Theorem 1) that are directly applicable to any member of the exponential family. The used probabilistic encoding, furthermore, allows for learning prior parameters. For the approach investigated here, we consequently argue that it represents the most flexible and most generally applicable latent variable model which has been suggested so far for exponential family observables. As such, it allows in principle for using many more distributions that have not been addressed previously including categorical, Dirichlet, normal-gamma etc. For multiple-parameter distributions, multiple matrices are used to couple latents to observables (see Fig. 1), and the same is the case for Gaussian observables (see Fig. 5). Preliminary example algorithms based on one- and two-parameter distributions of the exponential family suggest that feasible and competitive learning algorithms are obtained if the result derived here are applied. Furthermore, we have demonstrated scalability, e.g., by using approximate posteriors for efficient variational optimization (see Sec. 4.2).

Our example applications included structure finding in image patches, automatic estimation of

noise distributions (also compare [59] and [58]), and denoising of data subject to non-Gaussian noise. In the case of Poisson noise, where a number of alternative approaches are available, we observed competitive performance. In particular, denoising results improved on models which used Poisson noise with linear superposition: Non-Local Sparse Principal Component Analysis (NLSPCA) [27] and Sparse Poisson Denoising Algorithm (SPDA) [44]. Comparison to NLSPCA and SPDA may be particularly interesting in the context of this work. Both NLSPCA and SPDA use the standard coupling to observables via the natural parameter of the Poisson, whereas P-MCA sets the mean. Also, NLSPCA and SPDA use a linear superposition, while P-MCA uses the maximum. Comparison in Tab. 2 shows, in general, a better denoising performance of the P-MCA compared to both NLSPCA and SPDA. Poisson noise is just one example instance for which Theorem 1 applies and denoising is just one example application. That P-MCA is competitive for the task without further mechanisms (compare NLSPCA and SPDA) and without extensive fine-tuning may be taken as evidence in favor of the general approach derived here.

In analogy to the use of standard sparse coding, further application examples would include inpainting, compression, feature learning, or compressed sensing for data with in principle any exponential family noise distribution. Future work may also include the use of more richly structured prior distributions. As the derived update equations apply in general for any binary latents, the independent Bernoulli prior could be replaced by a deep model. Binary latents for deep generative graphical models are very common such that, e.g., deep SBNs [36, 37] but also deep restricted Boltzmann Machines [89] may be used.

**Acknowledgments.** This project was funded by the German Ministry of Research and Education (BMBF) in project 05M2020 (SPApplus, TP3, recipients HM and FH) and by the German Research Foundation (DFG) in projects 352015383 (HAPPAA, CRC 1330, B2, recipient JD) and 390895286 (cluster of excellence H4a 2.0, EXC 2177/1, recipient HM). Furthermore, we acknowledge support by the HPC Cluster CARL of Oldenburg University and by the HLRN network of HPC clusters (project nim00006).

## References

- [1] M. Tipping and C. Bishop, “Probabilistic principal component analysis,” *Journal of the Royal Statistical Society. Series B*, vol. 61, 1999.
- [2] S. Roweis, “EM algorithms for PCA and SPCA,” *NIPS*, pp. 626–32, 1998.
- [3] R. Cattell, *The scientific use of factor analysis in behavioral and life sciences*. Springer Science & Business Media, 2012.
- [4] B. Olshausen and D. Field, “Emergence of simple-cell receptive field properties by learning a sparse code for natural images,” *Nature*, vol. 381, pp. 607–9, 1996.
- [5] R. Tibshirani, “Regression shrinkage and selection via the lasso,” *J Royal Statistical Society. Series B*, vol. 58, no. 1, pp. 267–288, 1996.
- [6] P. Berkes, B. White, and J. Fiser, “No evidence for active sparsification in the visual cortex,” *Advances in Neural Information Processing Systems*, vol. 22, 2009.
- [7] M. Haft, R. Hofman, and V. Tresp, “Generative binary codes,” *Pattern Anal Appl*, vol. 6, pp. 269–84, 2004.



- [8] M. Henniges, G. Puertas, J. Bornschein, J. Eggert, and J. Lücke, “Binary sparse coding,” in *Proceedings LVA/ICA*, LNCS 6365, pp. 450–57, Springer, 2010.
- [9] G. Exarchakis and J. Lücke, “Discrete sparse coding,” *Neural Computation*, vol. 29, pp. 2979–3013, 2017.
- [10] M. K. Titsias and M. Lázaro-Gredilla, “Spike and slab variational inference for multi-task and multiple kernel learning,” in *Advances in Neural Information Processing Systems*, vol. 24, 2011.
- [11] I. Goodfellow, A. C. Courville, and Y. Bengio, “Large-scale feature learning with spike-and-slab sparse coding,” in *ICML*, 2012.
- [12] A.-S. Sheikh, J. A. Shelton, and J. Lücke, “A truncated EM approach for spike-and-slab sparse coding,” *Journal of Machine Learning Research*, vol. 15, pp. 2653–2687, 2014.
- [13] D. L. Donoho, “Compressed sensing,” *IEEE Transactions on information theory*, vol. 52, no. 4, pp. 1289–1306, 2006.
- [14] R. G. Baraniuk, “Compressive sensing,” *IEEE signal processing magazine*, vol. 24, no. 4, 2007.
- [15] A. B. Patel, T. Nguyen, and R. G. Baraniuk, “A probabilistic theory of deep learning,” in *Advances in Neural Information Processing Systems (NIPS)*, pp. 2558–2566, 2016.
- [16] W. Młynarski and J. H. McDermott, “Learning midlevel auditory codes from natural sound statistics,” *Neural computation*, vol. 30, no. 3, pp. 631–669, 2018.
- [17] J. Bornschein, M. Henniges, and J. Lücke, “Are V1 receptive fields shaped by low-level visual occlusions? A comparative study,” *PLOS Computational Biology*, vol. 9, no. 6, p. e1003062, 2013.
- [18] S. T. Roweis, “Factorial models and refiltering for speech separation and denoising,” in *Proc. Eurospeech*, vol. 7, pp. 1009 – 1012, 2003.
- [19] J. Lücke and M. Sahani, “Maximal causes for non-linear component extraction,” *Journal of Machine Learning Research*, vol. 9, pp. 1227–67, 2008.
- [20] A.-S. Sheikh, N. S. Harper, J. Drefs, Y. Singer, Z. Dai, R. E. Turner, and J. Lücke, “STRFs in primary auditory cortex emerge from masking-based statistics of natural sounds,” *PLoS computational biology*, vol. 15, no. 1, p. e1006595, 2019.
- [21] A. Hyvärinen and P. Pajunen, “Nonlinear Independent Component Analysis: Existence and uniqueness results,” *Neural Networks*, vol. 12, no. 3, pp. 429–439, 1999.
- [22] A. Hyvarinen, H. Sasaki, and R. Turner, “Nonlinear ICA using auxiliary variables and generalized contrastive learning,” in *The 22nd International Conference on Artificial Intelligence and Statistics*, pp. 859–868, 2019.
- [23] A. Hyvarinen and H. Morioka, “Nonlinear ICA of temporally dependent stationary sources,” *Proceedings of Machine Learning Research*, 2017.
- [24] P. Dayan and L. F. Abbott, *Theoretical Neuroscience*. MIT Press, Cambridge, 2001.

- [25] G. Puertas, J. Bornschein, and J. Lücke, “The maximal causes of natural scenes are edge filters,” in *Advances in Neural Information Processing Systems*, vol. 23, pp. 1939–1947, 2010.
- [26] M. Zhou, L. Hannah, D. Dunson, and L. Carin, “Beta-negative binomial process and poisson factor analysis,” in *Artificial Intelligence and Statistics*, pp. 1462–1471, 2012.
- [27] J. Salmon, Z. Harmany, C.-A. Deledalle, and R. Willett, “Poisson noise reduction with non-local PCA,” *Journal of mathematical imaging and vision*, vol. 48, no. 2, pp. 279–294, 2014.
- [28] M. Collins, S. Dasgupta, and R. E. Schapire, “A generalization of principal components analysis to the exponential family,” in *Advances in neural information processing systems*, pp. 617–624, 2002.
- [29] S. Mohamed, Z. Ghahramani, and K. A. Heller, “Bayesian exponential family PCA,” in *Advances in neural information processing systems*, pp. 1089–1096, 2009.
- [30] M. D. Hoffman, “Poisson-uniform nonnegative matrix factorization,” in *Acoustics, Speech and Signal Processing (ICASSP), 2012 IEEE International Conference on*, pp. 5361–5364, IEEE, 2012.
- [31] H. Lee, R. Raina, A. Teichman, and A. Y. Ng, “Exponential family sparse coding with application to self-taught learning,” in *IJCAI*, vol. 9, pp. 1113–1119, 2009.
- [32] J. Lücke and J. Eggert, “Expectation truncation and the benefits of preselection in training generative models,” *Journal of Machine Learning Research*, vol. 11, pp. 2855–900, 2010.
- [33] T. Šingliar and M. Hauskrecht, “Noisy-OR component analysis and its application to link analysis,” *Journal of Machine Learning Research*, vol. 7, pp. 2189–2213, Dec. 2006.
- [34] Y. Jernite, Y. Halpern, and D. Sontag, “Discovering hidden variables in noisy-or networks using quartet tests,” in *NIPS 26*, MIT Press, 2013.
- [35] A. A. Frolov, D. Husek, and P. Y. Polyakov, “Two expectation-maximization algorithms for boolean factor analysis,” *Neurocomputing*, vol. 130, no. 0, pp. 83 – 97, 2014.
- [36] L. K. Saul, T. Jaakkola, and M. I. Jordan, “Mean field theory for sigmoid belief networks,” *Journal of artificial intelligence research*, vol. 4, no. 1, pp. 61–76, 1996.
- [37] Z. Gan, R. Henao, D. Carlson, and L. Carin, “Learning Deep Sigmoid Belief Networks with Data Augmentation,” in *AISTATS*, 2015.
- [38] W. J. van der Linden and R. K. Hambleton, *Handbook of modern item response theory*. Springer Science & Business Media, 2013.
- [39] R. T. Rockafellar and R. J.-B. Wets, *Variational analysis*, vol. 317. Springer Science & Business Media, 2009.
- [40] D. R. Cox, *Principles of statistical inference*. Cambridge university press, 2006.
- [41] M. J. Wainwright, M. I. Jordan, *et al.*, “Graphical models, exponential families, and variational inference,” *Foundations and Trends® in Machine Learning*, vol. 1, no. 1–2, pp. 1–305, 2008.
- [42] S. Mohamed, K. Heller, and Z. Ghahramani, “Sparse exponential family latent variable models,” in *NIPS Workshop*, 2010.

- [43] S. Mohamed, K. Heller, and Z. Ghahramani, “Bayesian and l1 approaches to sparse unsupervised learning,” *arXiv preprint arXiv:1106.1157*, 2011.
- [44] R. Giryes and M. Elad, “Sparsity-based poisson denoising with dictionary learning,” *IEEE Transactions on Image Processing*, vol. 23, no. 12, pp. 5057–5069, 2014.
- [45] M. Lu, J. Z. Huang, and X. Qian, “Sparse exponential family principal component analysis,” *Pattern recognition*, vol. 60, pp. 681–691, 2016.
- [46] M. E. E. Khan, G. Bouchard, K. P. Murphy, and B. M. Marlin, “Variational bounds for mixed-data factor analysis,” in *Advances in Neural Information Processing Systems*, pp. 1108–1116, 2010.
- [47] S. H. Mousavi, J. Drefs, and J. Lücke, “A double-dictionary approach learns component means and variances for V1 encoding,” in *The Sixth International Conference on Machine Learning, Optimization and Data Science (LOD)*, Springer, 2020.
- [48] R. Neal and G. Hinton, “A view of the EM algorithm that justifies incremental, sparse, and other variants,” in *Learning in Graphical Models* (M. I. Jordan, ed.), Kluwer, 1998.
- [49] J. D. McAuliffe and D. M. Blei, “Supervised topic models,” in *Advances in neural information processing systems*, pp. 121–128, 2008.
- [50] A. P. Dempster, N. M. Laird, and D. B. Rubin, “Maximum likelihood from incomplete data via the EM algorithm (with discussion),” *Journal of the Royal Statistical Society B*, vol. 39, pp. 1–38, 1977.
- [51] E. Guiraud, J. Drefs, and J. Lücke, “Evolutionary expectation maximization,” in *Proceedings of the Genetic and Evolutionary Computation Conference*, pp. 442–449, ACM, 2018.
- [52] J. Lücke, “Truncated variational expectation maximization,” *arXiv*, vol. 1610, 2017.
- [53] P. Földiák, “Forming sparse representations by local anti-Hebbian learning,” *Biological Cybernetics*, vol. 64, pp. 165–170, 1990.
- [54] M. W. Spratling, “Pre-synaptic lateral inhibition provides a better architecture for self-organising neural networks,” *Network: Computation in Neural Systems*, vol. 10, pp. 285 – 301, 1999.
- [55] J. A. Shelton, J. Gasthaus, Z. Dai, J. Lücke, and A. Gretton, “GP-select: Accelerating em using adaptive subspace preselection,” *Neural Computation*, vol. 29, no. 8, pp. 2177–2202, 2017. 1st version, arXiv:1412.3411, online since 2014.
- [56] J. H. van Hateren and A. van der Schaaf, “Independent component filters of natural images compared with simple cells in primary visual cortex,” *Proceedings of the Royal Society of London B*, vol. 265, pp. 359–66, 1998.
- [57] A. Teymurazyan, T. Riauka, H.-S. Jans, and D. Robinson, “Properties of noise in positron emission tomography images reconstructed with filtered-backprojection and row-action maximum likelihood algorithm,” *Journal of digital imaging*, vol. 26, no. 3, pp. 447–456, 2013.
- [58] I. Valera and Z. Ghahramani, “Automatic discovery of the statistical types of variables in a dataset,” in *International Conference on Machine Learning*, pp. 3521–3529, 2017.

- [59] A. Vergari, A. Molina, R. Peharz, Z. Ghahramani, K. Kersting, and I. Valera, “Automatic bayesian density analysis,” in *Proceedings of the AAAI Conference on Artificial Intelligence*, vol. 33, pp. 5207–5215, 2019.
- [60] D. J. C. MacKay, *Information Theory, Inference, and Learning Algorithms*. Cambridge University Press, 2003. Available from <http://www.inference.phy.cam.ac.uk/mackay/itila/>.
- [61] K. Dabov, A. Foi, V. Katkovnik, and K. Egiazarian, “Image denoising by sparse 3d transform-domain collaborative filtering,” *IEEE Transactions on Image Processing*, vol. 16, no. 8, pp. 2080–2095, 2007.
- [62] S. Gu, L. Zhang, W. Zuo, and X. Feng, “Weighted nuclear norm minimization with application to image denoising,” in *Proceedings of the IEEE Conference on Computer Vision and Pattern Recognition*, pp. 2862–2869, 2014.
- [63] H. C. Burger, C. J. Schuler, and S. Harmeling, “Image denoising: Can plain neural networks compete with BM3D?,” in *Proceedings of the IEEE Conference on Computer Vision and Pattern Recognition*, pp. 2392–2399, 2012.
- [64] S. Chaudhury and H. Roy, “Can fully convolutional networks perform well for general image restoration problems?,” in *2017 Fifteenth IAPR International Conference on Machine Vision Applications (MVA)*, pp. 254–257, IEEE, 2017.
- [65] Y. Chen and T. Pock, “Trainable nonlinear reaction diffusion: A flexible framework for fast and effective image restoration,” *IEEE Transactions on Pattern Analysis and Machine Intelligence*, vol. 39, no. 6, pp. 1256–1272, 2017.
- [66] K. Zhang, W. Zuo, Y. Chen, D. Meng, and L. Zhang, “Beyond a gaussian denoiser: Residual learning of deep cnn for image denoising,” *IEEE Transactions on Image Processing*, vol. 26, no. 7, pp. 3142–3155, 2017.
- [67] Y. Tai, J. Yang, X. Liu, and C. Xu, “Memnet: A persistent memory network for image restoration,” in *Proceedings of the IEEE international conference on computer vision*, pp. 4539–4547, 2017.
- [68] K. Zhang, W. Zuo, and L. Zhang, “FFDNet: Toward a fast and flexible solution for cnn-based image denoising,” *IEEE Transactions on Image Processing*, vol. 27, no. 9, pp. 4608–4622, 2018.
- [69] A. Tarantola, *Inverse problem theory and methods for model parameter estimation*. SIAM, 2005.
- [70] A. Shocher, N. Cohen, and M. Irani, ““zero-shot” super-resolution using deep internal learning,” in *Proceedings of the IEEE conference on computer vision and pattern recognition*, pp. 3118–3126, 2018.
- [71] R. Imamura, T. Itasaka, and M. Okuda, “Zero-shot hyperspectral image denoising with separable image prior,” in *Proceedings of the IEEE International Conference on Computer Vision Workshops*, pp. 0–0, 2019.
- [72] K. Dabov, A. Foi, V. Katkovnik, and K. Egiazarian, “Image denoising by sparse 3-d transform-domain collaborative filtering,” *IEEE Transactions on image processing*, vol. 16, no. 8, pp. 2080–2095, 2007.

- [73] M. Aharon, M. Elad, and A. Bruckstein, “K-SVD: An algorithm for designing overcomplete dictionaries for sparse representation,” *IEEE Transactions on signal processing*, vol. 54, no. 11, pp. 4311–4322, 2006.
- [74] F. J. Anscombe, “The transformation of poisson, binomial and negative-binomial data,” *Biometrika*, vol. 35, no. 3/4, pp. 246–254, 1948.
- [75] M. Fisz, “The limiting distribution of a function of two independent random variables and its statistical application,” in *Colloquium Mathematicum*, vol. 3, pp. 138–146, 1955.
- [76] M. Makitalo and A. Foi, “Optimal inversion of the anscombe transformation in low-count poisson image denoising,” *IEEE transactions on Image Processing*, vol. 20, no. 1, pp. 99–109, 2010.
- [77] A. Rond, R. Giryes, and M. Elad, “Poisson inverse problems by the plug-and-play scheme,” *arXiv:1511.02500*, later in *J. of Visual Communication and Image Representation*, vol. 41, pp. 96–108, 2016.
- [78] L. Azzari and A. Foi, “Variance stabilization for noisy+ estimate combination in iterative poisson denoising,” *IEEE signal processing letters*, vol. 23, no. 8, pp. 1086–1090, 2016.
- [79] M. Niknejad and M. A. Figueiredo, “Poisson image denoising using best linear prediction: A post-processing framework,” in *2018 26th European Signal Processing Conference (EUSIPCO)*, pp. 2230–2234, IEEE, 2018.
- [80] T. Remez, O. Litany, R. Giryes, and A. M. Bronstein, “Deep convolutional denoising of low-light images,” *arXiv preprint arXiv:1701.01687*, 2017.
- [81] W. Kumwilaisak, T. Piriyaarawat, P. Lasang, and N. Thatphithakkul, “Image denoising with deep convolutional neural and multi-directional long short-term memory networks under poisson noise environments,” *IEEE Access*, vol. 8, pp. 86998–87010, 2020.
- [82] O. DeGuchy, F. Santiago, M. Banuelos, and R. F. Marcia, “Deep neural networks for low-resolution photon-limited imaging,” in *ICASSP 2019-2019 IEEE International Conference on Acoustics, Speech and Signal Processing (ICASSP)*, pp. 3247–3251, IEEE, 2019.
- [83] T. Piriyaarawat, W. Kumwilaisak, and P. Lasang, “Image denoising with deep convolutional and multi-directional LSTM networks under poisson noise environments,” in *2018 18th International Symposium on Communications and Information Technologies (ISCIT)*, pp. 90–95, IEEE, 2018.
- [84] Q. Jin, O. Miyashita, F. Tama, J. Yang, and S. Jonic, “Poisson image denoising by piecewise principal component analysis and its application in single-particle x-ray diffraction imaging,” *IET Image Processing*, vol. 12, no. 12, pp. 2264–2274, 2018.
- [85] I. Goodfellow, A. C. Courville, and Y. Bengio, “Spike-and-slab sparse coding for unsupervised feature discovery,” in *NIPS Workshop on Challenges in Learning Hierarchical Models: Transfer Learning and Optimization*, 2011.
- [86] D. D. Lee and H. S. Seung, “Learning the parts of objects by non-negative matrix factorization,” *Nature*, vol. 401, no. 6755, pp. 788–91, 1999.
- [87] T. Singliar and M. Hauskrecht, “Noisy-OR component analysis and its application to link analysis,” *JMLR*, pp. 2189–2213, 2006.

- [88] A. A. Frolov, D. Húsek, and P. Y. Polyakov, “Comparison of seven methods for boolean factor analysis and their evaluation by information gain,” *IEEE transactions on neural networks and learning systems*, vol. 27, no. 3, pp. 538–550, 2015.
- [89] H. Larochelle and Y. Bengio, “Classification using discriminative restricted Boltzmann machines,” in *Proceedings of the 25th international conference on Machine learning*, pp. 536–543, ACM, 2008.
- [90] M. Spratling, “Learning image components for object recognition,” *Journal of Machine Learning Research*, vol. 7, pp. 793–815, 2006.
- [91] T. Mou, J. Huang, and F. O’Sullivan, “The gamma characteristic of reconstructed PET images: Implications for ROI analysis,” *IEEE Transactions on Medical Imaging*, vol. 37, no. 5, pp. 1092–1102, 2018.

## Appendix

### A Additional Details on Parameter Update Equations

#### A.1 Parameter Update Equations – General Case

We derived Theorem 1 for the case of  $L = 2$ , i.e., for distributions of the exponential family with sufficient statistics  $\vec{T}(y)$  of length two. This choice was for notational convenience only. Considering the proof of Theorem 1, it can easily be inferred that it applies for any  $L$ . We state this more formally in the following:

Instead of two matrices  $W$  and  $V$ , we consider in general  $L$  matrices, which we will denote by  $W^{(1)}$  to  $W^{(L)}$ . Therefore, we have to generalize our definition of  $\vec{\eta}_d(\vec{s}, \Theta)$ , which is now given by:

$$\vec{\eta}_d(\vec{s}, \Theta) := \vec{\Phi}(\bar{W}_d^{(1)}(\vec{s}, \Theta), \dots, \bar{W}_d^{(L)}(\vec{s}, \Theta)). \quad (44)$$

Given matrices  $W^{(1)}, \dots, W^{(L)} \in \mathbb{R}^{D \times H}$  we now have to define the mappings  $W_d^{(l)}(\vec{s}, \Theta)$  for  $l = 1, \dots, L$ . In analogy to the  $L = 2$  case, we do so again by first defining a matrix  $M(\Theta) \in \mathbb{R}^{D \times H}$ :

$$\forall d, h : \quad M_{dh}(\Theta) = F(W_{dh}^{(1)}, \dots, W_{dh}^{(L)}) \quad \text{with} \quad F(\vec{w}) = \langle y \rangle_{p(y; \vec{\Phi}(\vec{w}))}. \quad (45)$$

Using matrix  $M(\Theta)$  we now define our mappings  $\bar{W}_d^{(l)}(\vec{s}, \Theta)$  as follows:

$$\forall l, d, h : \quad \bar{W}_d^{(l)}(\vec{s}, \Theta) := W_{dh}^{(l)} \quad \text{with} \quad h(d, \vec{s}, \Theta) := \operatorname{argmax}_h \{M_{dh}(\Theta) s_h\}. \quad (46)$$

Also in the general case, the definitions (45) and (46) guarantee that the mean of observable  $d$  is given by  $\mu_d = \max_h \{M_{dh}(\Theta) s_h\}$ .

As the function  $\vec{\eta}_d(\vec{s}, \Theta)$  models the influence of the latent variables on the observed variables, it is reminiscent of the link functions as, e.g., defined for generalized linear regression. Furthermore, our definitions (44) to (46) ensure that the means  $\mu_d$  of the observables are always given by a superposition defined by matrix  $M(\Theta)$ , which is likewise reminiscent of the link functions

for non-linear regression. Our definition of  $\vec{\eta}_d(\vec{s}, \Theta)$  via  $M(\Theta)$  is less direct as we use a maximum superposition, which notably differs from usual definitions of link functions (alongside other technical differences). The general role of coupling observables to latent variables (or response variables in regression) is also played by  $\vec{\eta}_d(\vec{s}, \Theta)$  such that it may in a broader sense be referred to as a link function as well.

Now, for the equations (6)-(8) with (44) to (46) that generally define the family of ef-MCA data models, the following general theorem applies:

**Theorem 2** Consider an ef-MCA data model (6) to (8) with  $p(y; \vec{\eta})$  being an exponential family distribution with sufficient statistics vector  $\vec{T}(y)$  of length  $L \in \mathbb{N}$ . Let the parameters  $\Theta$  contain  $L$  matrices  $W^{(1)}, \dots, W^{(L)} \in \mathbb{R}^{D \times H}$  and let  $\vec{\eta}_d(\vec{s}, \Theta)$  be defined as in Eqns. (44) to (46). Then

the derivatives of the variational lower bound (23) w.r.t. all  $W_{dh}^{(l)}$  are zero if for all  $d, h$ , and  $l$  applies:

$$W_{dh}^{(l)} = \frac{\sum_{n=1}^N \langle \mathcal{A}_{dh}(\vec{s}, \Theta) \rangle_{q^{(n)}} T_l(y_d^{(n)})}{\sum_{n=1}^N \langle \mathcal{A}_{dh}(\vec{s}, \Theta) \rangle_{q^{(n)}}}. \quad (47)$$

where  $\mathcal{A}_{dh}(\vec{s}, \Theta)$  is given by (26).

**Proof 3** Consider a single parameter  $W_{dh}^{(l)}$  for an arbitrary  $1 \leq l \leq L$  and, for better readability, let us abbreviate  $\bar{W}_d^{(1)} = \bar{W}_d^{(1)}(\vec{s}, \Theta)$  to  $\bar{W}_d^{(L)} = \bar{W}_d^{(L)}(\vec{s}, \Theta)$ . Then using the chain rule, we get

$$\begin{aligned} \frac{\partial}{\partial W_{dh}^{(l)}} \log(p(y_d; \vec{\eta}_d(\vec{s}, \Theta))) &= \frac{\partial}{\partial W_{dh}^{(l)}} \log(p(y_d; \vec{\Phi}(\bar{W}_d^{(1)}, \dots, \bar{W}_d^{(L)}))) \\ &= \sum_{l=1}^L \left( \frac{\partial}{\partial W_{dh}^{(l)}} \Phi_l(\bar{W}_d^{(1)}, \dots, \bar{W}_d^{(L)}) \right) \left( \frac{\partial}{\partial \eta_l} \log(p(y_d; \vec{\eta})) \Big|_{\vec{\eta}=\vec{\Phi}(\bar{W}_d^{(1)}, \dots, \bar{W}_d^{(L)})} \right) \\ &= \sum_{l=1}^L \left( \frac{\partial}{\partial W_{dh}^{(l)}} \bar{W}_d^{(l)} \right) \left( \frac{\partial}{\partial w} \Phi_l(\bar{W}_d^{(1)}, \dots, w, \dots, \bar{W}_d^{(L)}) \Big|_{w=\bar{W}_d^{(l)}} \right) \\ &\quad \times \left( \frac{\partial}{\partial \eta_l} \log(p(y_d; \vec{\eta})) \Big|_{\vec{\eta}=\vec{\Phi}(\bar{W}_d^{(1)}, \dots, \bar{W}_d^{(L)})} \right) \\ &= \sum_{l=1}^L \left( \mathcal{A}_{dh}(\vec{s}, \Theta) \right) \left( \frac{\partial}{\partial w} \Phi_l(\bar{W}_d^{(1)}, \dots, w, \dots, \bar{W}_d^{(L)}) \Big|_{w=\bar{W}_d^{(l)}} \right) \\ &\quad \times \left( T_l(y_d^{(n)}) - \frac{\partial A(\vec{\eta})}{\partial \eta_l} \Big|_{\vec{\eta}=\vec{\Phi}(\bar{W}_d^{(1)}, \dots, \bar{W}_d^{(L)})} \right). \end{aligned} \quad (48)$$

Moreover, we know that for any distribution of the exponential family,  $A(\vec{\eta})$  for  $l = 1, \dots, L$  satisfies (see [41] for more information):

$$\frac{\partial A(\vec{\eta})}{\partial \eta_l} = \langle T_l(y) \rangle_{p(y; \vec{\eta})} \quad (49)$$

(for finite  $A(\vec{\eta})$ ) which results in

$$\begin{aligned}
\frac{\partial}{\partial W_{dh}^{(l)}} \log(p(y_d; \vec{\eta}_d(\vec{s}, \Theta))) &= \sum_{l=1}^L \left( \mathcal{A}_{dh}(\vec{s}, \Theta) \right) \left( \frac{\partial}{\partial w} \Phi_l(\bar{W}_d^{(1)}, \dots, w, \dots, \bar{W}_d^{(L)}) \Big|_{w=\bar{W}_d^{(l)}} \right) \\
&\quad \times \left( T_l(y_d^{(n)}) - \langle T_l(y) \rangle_{p(y; \vec{\eta})} \right) \Big|_{\vec{\eta}=\vec{\Phi}(\bar{W}_d^{(1)}, \dots, \bar{W}_d^{(L)})} \\
&= \sum_{l=1}^L \left( \mathcal{A}_{dh}(\vec{s}, \Theta) \right) \left( \frac{\partial}{\partial w} \Phi_l(\bar{W}_d^{(1)}, \dots, w, \dots, \bar{W}_d^{(L)}) \Big|_{w=\bar{W}_d^{(l)}} \right) \\
&\quad \times \left( T_l(y_d^{(n)}) - \langle T_l(y) \rangle_{p(y; \vec{\Phi}(\bar{W}_d^{(1)}, \dots, \bar{W}_d^{(L)}))} \right). \tag{50}
\end{aligned}$$

Now, using Lemma 1 we obtain

$$\begin{aligned}
\frac{\partial}{\partial W_{dh}^{(l)}} \log(p(y_d; \vec{\eta}_d(\vec{s}, \Theta))) &= \sum_{l=1}^L \left( \mathcal{A}_{dh}(\vec{s}, \Theta) \right) \left( \frac{\partial}{\partial w} \Phi_l(W_{dh}^{(1)}, \dots, w, \dots, W_{dh}^{(L)}) \Big|_{w=W_{dh}^{(l)}} \right) \\
&\quad \times \left( T_l(y_d^{(n)}) - \langle T_l(y) \rangle_{p(y; \vec{\Phi}(W_{dh}^{(1)}, \dots, W_{dh}^{(L)}))} \right). \tag{51}
\end{aligned}$$

Note that above equation depends on parameter  $\vec{s}$  of the hidden states only through function  $\mathcal{A}_{dh}(\vec{s}, \Theta)$ . We then have

$$\begin{aligned}
\frac{\partial}{\partial W_{dh}^{(l)}} \mathcal{F}(q, \Theta) &= \sum_n \sum_{\vec{s}} q^{(n)}(\vec{s}) \frac{\partial}{\partial W_{dh}^{(l)}} \log(p(y_d^{(n)}; \vec{\eta}_d(\vec{s}, \Theta))) \\
&= \sum_n \sum_{\vec{s}} q^{(n)}(\vec{s}) \sum_{l=1}^L \left( \mathcal{A}_{dh}(\vec{s}, \Theta) \right) \left( \frac{\partial}{\partial w} \Phi_l(W_{dh}^{(1)}, \dots, w, \dots, W_{dh}^{(L)}) \Big|_{w=W_{dh}^{(l)}} \right) \\
&\quad \times \left( T_l(y_d^{(n)}) - \langle T_l(y) \rangle_{p(y; \vec{\Phi}(W_{dh}^{(1)}, \dots, W_{dh}^{(L)}))} \right) \\
&= \sum_{l=1}^L \left( \frac{\partial}{\partial w} \Phi_l(W_{dh}^{(1)}, \dots, w, \dots, W_{dh}^{(L)}) \Big|_{w=W_{dh}^{(l)}} \right) \sum_n \langle \mathcal{A}_{dh} \rangle_{q^{(n)}} \\
&\quad \times \left( T_l(y_d^{(n)}) - W_{dh}^{(l)} \right)
\end{aligned} \tag{52}$$

where in the last equation we exploited our mean value parameterization defined in (4) that is

$$\vec{w} := \langle \vec{T}(y) \rangle_{p(y; \vec{\eta})}. \tag{53}$$

Therefore, independently of the choice of functions  $\frac{\partial}{\partial w} \Phi_l(W_{dh}^{(1)}, \dots, w, \dots, W_{dh}^{(L)}) \Big|_{w=W_{dh}^{(l)}}$  for

each  $l$ ,  $\frac{\partial \mathcal{F}}{\partial W_{dh}^{(l)}} = 0$  if, for  $l = 1, \dots, L$ , we set

$$\sum_n \langle \mathcal{A}_{dh}(\vec{s}, \Theta) \rangle_{q^{(n)}} (T_l(y_d^{(n)}) - W_{dh}^{(l)}) = 0 \tag{54}$$



that yields equation (47) and completes the proof.  $\square$

The general case does, of course, also include the  $L = 1$  case and consequently Bernoulli, Exponential or the Poisson distribution.

## A.2 Parameterization of the Gaussian-MCA

For Gaussian-MCA (G-MCA) in Example 2, the generative model was shown to be given by:

$$p(\vec{s} | \Theta) = \prod_{h=1}^H \pi_h^{s_h} (1 - \pi_h)^{1-s_h} \quad (55)$$

$$p(\vec{y} | \vec{s}, \Theta) = \prod_{d=1}^D \mathcal{N}(y_d; \bar{W}_d(\vec{s}, \Theta), \bar{V}_d(\vec{s}, \Theta) - \bar{W}_d^2(\vec{s}, \Theta)) \quad (56)$$

where we can use the update equations of Theorem 1 for  $W$  and  $V$ . To obtain some intuition, we can also define the function:

$$\bar{\sigma}_d^2(\vec{s}, \Theta) = \bar{V}_d(\vec{s}, \Theta) - \bar{W}_d^2(\vec{s}, \Theta), \quad \forall d.$$

Because of the definition of  $\bar{W}_d(\vec{s}, \Theta)$  and  $\bar{V}_d(\vec{s}, \Theta)$  in (20) we get:

$$\bar{\sigma}_d^2(\vec{s}, \Theta) = \sigma_{dh(d, \vec{s}, \Theta)}^2 \text{ where } h(d, \vec{s}, \Theta) = \operatorname{argmax}_h \{W_{dh}s_h\} \text{ and } \sigma_{dh}^2 = V_{dh} - W_{dh}^2.$$

The generative model then becomes:

$$p(\vec{s} | \Theta) = \prod_{h=1}^H \pi_h^{s_h} (1 - \pi_h)^{1-s_h} \quad (57)$$

$$p(\vec{y} | \vec{s}, \Theta) = \prod_{d=1}^D \mathcal{N}(y_d; \bar{W}_d(\vec{s}, \Theta), \bar{\sigma}_d^2(\vec{s}, \Theta)) \quad (58)$$

The latents thus change the mean via the matrix  $W$  and the variance via the matrices  $V$  and  $W$ . We can now use the update rules for  $V_{dh}$  and  $W_{dh}$  and compute the matrices  $\sigma_{dh}^2$  as a result. Alternatively, we can also combine the update rules for  $V_{dh}$  and  $W_{dh}$  to directly obtain an update rule for  $\sigma_{dh}^2$ :

$$\begin{aligned} (\sigma_{dh}^2)^{\text{new}} &= V_{dh}^{\text{new}} - (W_{dh}^{\text{new}})^2 = V_{dh}^{\text{new}} - 2 W_{dh}^{\text{new}} W_{dh}^{\text{new}} + (W_{dh}^{\text{new}})^2 \\ &= \frac{\sum_{n=1}^N \langle \mathcal{A}_{dh}(\vec{s}, \Theta) \rangle_{q^{(n)}} (y_d^{(n)})^2}{\sum_{n=1}^N \langle \mathcal{A}_{dh}(\vec{s}, \Theta) \rangle_{q^{(n)}}} - 2 \frac{\sum_{n=1}^N \langle \mathcal{A}_{dh}(\vec{s}, \Theta) \rangle_{q^{(n)}} y_d^{(n)}}{\sum_{n=1}^N \langle \mathcal{A}_{dh}(\vec{s}, \Theta) \rangle_{q^{(n)}}} W_{dh}^{\text{new}} + (W_{dh}^{\text{new}})^2 \\ &= \frac{\sum_{n=1}^N \langle \mathcal{A}_{dh}(\vec{s}, \Theta) \rangle_{q^{(n)}} ((y_d^{(n)})^2 - 2 y_d^{(n)} W_{dh}^{\text{new}} + (W_{dh}^{\text{new}})^2)}{\sum_{n=1}^N \langle \mathcal{A}_{dh}(\vec{s}, \Theta) \rangle_{q^{(n)}}} \\ &= \frac{\sum_{n=1}^N \langle \mathcal{A}_{dh}(\vec{s}, \Theta) \rangle_{q^{(n)}} (y_d^{(n)} - W_{dh}^{\text{new}})^2}{\sum_{n=1}^N \langle \mathcal{A}_{dh}(\vec{s}, \Theta) \rangle_{q^{(n)}}}. \end{aligned} \quad (59)$$

This form of update is more familiar as it evaluates the square deviation from the mean given by  $W_{dh}^{\text{new}}$ . Also note that we first have to compute  $W_{dh}^{\text{new}}$  before updating  $\sigma_{dh}^2$ , which is in analogy, e.g., to standard Gaussian mixtures for variance (or covariance) updates. For the G-MCA application of Sec. 4.2, we show the matrices  $W_{dh}$  and  $\sigma_{dh}^2$  for whitened natural image patches.

### A.3 Second-Moment Update of the Gamma-MCA

Consider the Gamma distribution to be the noise of observables in the model (6)-(8), i.e. let:

$$p(\vec{y}|\vec{s}, \Theta) = \prod_{d=1}^D \text{Gamma}(y_d; \vec{\eta}_d(\vec{s}, \Theta)) \quad \text{for } y_d \in (0, \infty), \forall d. \quad (60)$$

Given the shape and rate parameters  $\alpha, \beta > 0$  of the Gamma distribution, the natural parameters and sufficient statistics are given by:

$$\vec{\eta} = (\alpha - 1, -\beta)^T, \quad \vec{T}(y_d) = (y_d, \log(y_d))^T. \quad (61)$$

Further, based on the mean value parameterization in (4) and (20), we have

$$\bar{W}(\vec{s}, \Theta) = \langle y \rangle_{p(y; \vec{\eta})}, \quad \bar{V}(\vec{s}, \Theta) = \langle \log(y) \rangle_{p(y; \vec{\eta})} \quad (62)$$

where  $\langle y \rangle_{p(y; \vec{\eta})}$  represents the mean of observables and equals to  $\frac{\eta_1 + 1}{-\eta_2}$ . Also for any  $y \in (0, \infty)$  we have

$$\langle \log(y) \rangle_{p(y; \vec{\eta})} = \psi(\eta_1 + 1) - \log(-\eta_2) \quad (63)$$

with the Digamma function  $\psi(\cdot)$  defined by:

$$\begin{aligned} \psi(x) &= \frac{d}{dx} \log(\Gamma(x)) = \log(x) - \frac{1}{2x} - \frac{1}{12x^2} + \dots \\ &= \log(x) - \frac{1}{2x} - \sum_{n=1}^{\infty} \frac{B_{2n}}{2nx^{2n}} \end{aligned} \quad (64)$$

where  $B_{2n} = (1, \frac{-1}{2}, \frac{1}{6}, \frac{-1}{30}, \dots)$  are the Bernoulli numbers. In short, we can write

$$\vec{w} = \begin{pmatrix} \bar{W} \\ \bar{V} \end{pmatrix} = \begin{pmatrix} \frac{\eta_1 + 1}{-\eta_2} \\ \psi(\eta_1 + 1) - \log(-\eta_2) \end{pmatrix}. \quad (65)$$

In order to compute the function  $\vec{\Phi}$ , substitute  $\eta_2 = \frac{\eta_1+1}{-\bar{W}}$  from the first equation into the second one to get:

$$\begin{aligned}\bar{V} &= \log(\eta_1 + 1) - \frac{1}{2(\eta_1 + 1)} - \sum_{n=1}^{\infty} \frac{B_{2n}}{2n(\eta_1 + 1)^{2n}} - \log\left(\frac{\eta_1 + 1}{\bar{W}}\right) \\ &= -\frac{1}{2(\eta_1 + 1)} - \sum_{n=1}^{\infty} \frac{B_{2n}}{2n(\eta_1 + 1)^{2n}} + \log(\bar{W}) \\ &\approx -\frac{1}{2(\eta_1 + 1)} + \log(\bar{W})\end{aligned}\quad (66)$$

where we approximated the Digamma function with its first two terms above. Thereby we obtain

$$\eta_1 \approx \frac{1}{2(\log(\bar{W}) - \bar{V})} - 1 \quad \text{and} \quad \eta_2 \approx \frac{-1}{2\bar{W}(\log(\bar{W}) - \bar{V})}. \quad (67)$$

Note that we only considered the first two terms of the Digamma function for mathematical convenience. However, the approximation can be further improved by considering more terms of the summation in (66). Having the natural parameters in (67), one can get

$$\vec{\eta}_d(\vec{s}, \Theta) = \vec{\Phi}(\bar{W}_d(\vec{s}, \Theta), \bar{V}_d(\vec{s}, \Theta)) \approx \left( \frac{\frac{1}{2(\log(\bar{W}_d(\vec{s}, \Theta)) - \bar{V}_d(\vec{s}, \Theta))} - 1}{\frac{-1}{2\bar{W}_d(\vec{s}, \Theta)(\log(\bar{W}_d(\vec{s}, \Theta)) - \bar{V}_d(\vec{s}, \Theta))}} \right).$$

Finally, for the Gamma distribution we have  $\sigma^2 = \frac{\eta_1+1}{\eta_2^2}$  that results in

$$\bar{\sigma}^2(\vec{s}, \Theta) \approx 2\bar{W}_d^2(\vec{s}, \Theta)(\log(\bar{W}_d(\vec{s}, \Theta)) - \bar{V}_d(\vec{s}, \Theta)), \quad \forall d \quad (68)$$

where

$$\bar{\sigma}_d^2(\vec{s}, \Theta) = \sigma_{dh(d, \vec{s}, \Theta)}^2 \quad \text{and} \quad h(d, \vec{s}, \Theta) = \operatorname{argmax}_h \{W_{dh} s_h\}. \quad (69)$$

Now, similar to the procedure presented above, we can obtain

$$\begin{aligned}(\sigma_{dh}^2)^{\text{new}} &\approx 2(W_{dh}^{\text{new}})^2 (\log(W_{dh}^{\text{new}}) - V_{dh}^{\text{new}}) \\ &\approx 2(W_{dh}^{\text{new}})^2 \left( \frac{\sum_{n=1}^N \langle \mathcal{A}_{dh}(\vec{s}, \Theta) \rangle_{q^{(n)}} \log(W_{dh}^{\text{new}})}{\sum_{n=1}^N \langle \mathcal{A}_{dh}(\vec{s}, \Theta) \rangle_{q^{(n)}}} - \frac{\sum_{n=1}^N \langle \mathcal{A}_{dh}(\vec{s}, \Theta) \rangle_{q^{(n)}} \log(y_d^{(n)})}{\sum_{n=1}^N \langle \mathcal{A}_{dh}(\vec{s}, \Theta) \rangle_{q^{(n)}}} \right) \\ &\approx 2 \frac{\sum_{n=1}^N \langle \mathcal{A}_{dh}(\vec{s}, \Theta) \rangle_{q^{(n)}} (W_{dh}^{\text{new}})^2 (\log(W_{dh}^{\text{new}}) - \log(y_d^{(n)}))}{\sum_{n=1}^N \langle \mathcal{A}_{dh}(\vec{s}, \Theta) \rangle_{q^{(n)}}}.\end{aligned}\quad (70)$$

The above equation can be used for updating the variance parameter of the Gamma-MCA model. Moreover, observe that despite the approximation of the Digamma function, in practice, the aforementioned equation provides a good estimation of the variance of the Gamma distribution. Other approximations of the Digamma function can be also used to improve the performance of the method. For the experiments above, however, we used the first three terms of the Digamma function in (64) for the approximation.

## B Experimental Settings

### B.1 The Bars Test

For the bars test presented in Sec.4.1, we set  $\pi_h^{gen} = \frac{2}{10}$  for  $h = 1, \dots, H$  (two active bars on average per data point) and generated  $N = 1000$  iid datapoints according to the presented ef-MCA model where the noise distribution is considered to be either Exponential or Bernoulli. The ground-truth parameter  $W$  of the E-MCA model was set to a value of 10 for the bars and 1 for the background, and 0.99 for the bars and 0.01 for the background of the B-MCA. Next, we trained E-MCA and B-MCA models on their corresponding data sets and updated their parameters using equations (39) and (41). For both algorithms, we initialized  $W$  by randomly choosing  $H$  datapoints and appending them to each other; also the values  $\pi_h$  were initialized at  $\frac{3}{10}$  for  $h = 1, \dots, H$ . We then performed 50 EM iterations. In each EM iteration, the M-step fixed-point equation (39) was (for simplicity) applied just once. In this context, one can also apply the fixed-point equations of the M-step different number of times to assess the convergence rate of the algorithms. Here, we observed similar behaviour of the E- and P-MCA algorithms when running the fixed-point equations multiple times compared to running it just once.

### B.2 Avoiding Local Optima

In our bars test experiments, we executed the algorithms multiple times while holding hyperparameters fixed and using different realizations of the initial model parameters in each run. We observed that the best solutions recovered all bars with high accuracy. In some cases, however, slight overfitting effects occurred that could be diminished by increasing the number of datapoints. We also frequently observed that the algorithms could not recover the ground-truth generative parameters. This can be seen as the effect of local optima which is different for each of the ef-MCA models. Local optima effects showed for instance to be more severe for the B-MCA algorithm compared to the P-MCA algorithm. While variational annealing schemes have frequently been applied as a measure against local optima effects, we here investigated an alternative approach in order to prevent the algorithm from converging to sub-optimal solutions. For these investigations, we used the Gamma-MCA as we observed the local optima effect to be sever for this model.

Concretely, we considered bars test data generated according to the Gamma-MCA model (Eqns. 6 and 60) and applied three different algorithms on this dataset: In the first and second case, we applied Gaussian- and Gamma-MCA separately. In the third case, we applied a Gamma-MCA model that we had initialized using the parameters learned by the Gaussian model. We refer to this latter approach as Gamma-MCA+. We considered two different scenarios and compared the log-likelihood values of the three algorithms (Gaussian-MCA, Gamma-MCA and Gamma-MCA+). In the first scenario, we initialized the model parameters of the Gaussian-MCA and of the Gamma-MCA model at the ground-truth values. In the second case, we used randomly initialized parameters instead. We then performed 10 runs of each algorithm using 100 EM iterations in each run. The results are depicted in Fig. 8. As the figure shows, when initializing the parameters at the ground-truth, the learned parameters tend to stay at the initial values which can be observed consistently for all models. Further, when initializing the parameters randomly, the Gamma-MCA+ model shows to achieve higher log-likelihood values in comparison to the other two models. The results of the Gamma-MCA model show that the model never achieves the optimal log-likelihood value. We can conclude that the Gamma-MCA+ approach helps alleviating the effect of local optima.

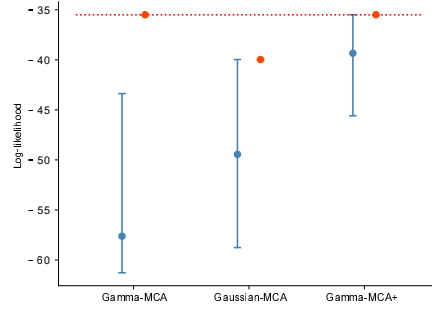


Figure 8: Comparison of the log-likelihood values for Gamma-MCA, Gaussian-MCA and Gamma-MCA+ algorithms trained on a dataset generated according to the Gamma-MCA model. Here, the red color denotes initializing the model parameters  $\Theta$  at ground-truth values and the blue corresponds to the random initialization. Moreover, the dots denote the average value of the log-likelihood values over 10 different runs; and further, the upper and lower bounds denote the maximum and minimum log-likelihoods achieved in these 10 runs. Finally, the red line presents the ground-truth log-likelihood value. As it can be seen, Gamma-MCA and Gamma-MCA+ have higher log-likelihoods at the optimum solution (red dots) rather than the Gaussian-MCA model which is the case for Gamma distributed data. Moreover, blue lines illustrate the effect of local optima for the Gamma-MCA model and also beneficiary of the Gamma-MCA+ model. That is, Gamma-MCA model never achieved the optimal log-likelihood value during these 10 runs and its results illustrate a clear local optima effect.

### B.3 Reliability For Binary Data

In addition to the local optima effect, the inherent complexity of the model can also affect its performance. That is, for instance, increasing the sparsity ( $\vec{\pi}H$ ) will decrease the reliability of the model. In fact, one measure that has been of interest is how robust an algorithm is w.r.t. the average number of active bars, and how often it reaches the global vs. any local optimum. The probability of recovering all bars has been termed "reliability" of the algorithm [90]. In the following, we further investigate the reliability of the Bernoulli-MCA (B-MCA) model for different levels of sparsity. For our purposes, we notably did not optimize learning to improve reliability (e.g., by introducing annealing procedures [32]) but used the canonical form of B-MCA with exact E-steps (i.e., full posteriors) and updated  $W$  and  $\vec{\pi}$  using Eqns. (39) and (41). We generated artificial datasets according to the B-MCA model similar to the procedure presented above with  $W_{dh} \in \{0.99, 0.01\}$  and varying values of  $\pi$  (we assumed  $\pi_h = \pi$  for  $h = 1, \dots, H$ ) that determine the average number of active bars per datapoint. For each value of  $\pi$ , we generated 200 different bars datasets each with  $N = 1000$  datapoints and then fitted a B-MCA model. We then computed 50 full EM iterations; initialization of  $W_{dh}$  and  $\pi$  were chosen as in the bars test experiments above. Reliability further measured in terms of the percentage of all trained B-MCA models that achieved a higher log-likelihood value than the ground-truth values (note that this is a good measure as the converged log-likelihoods are slightly higher than the ground-truth value due to the overfitting effect). Results are presented in Fig. 9.

As can be observed, the best runs always reach higher log-likelihood values than the generating parameters (due to slight overfitting). These runs do recover all bars patterns and the prior parameters. Even for values  $\pi = 0.5$ , i.e., for five out of ten bars per input on average, one to two out of 200 runs do extract all bars. The best runs in terms of log-likelihood can automatically be determined without knowledge of the ground-truth such that the resulting method would yield a

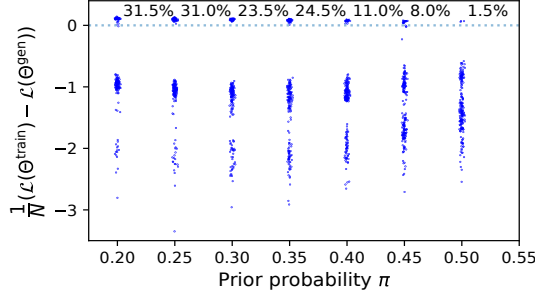


Figure 9: Differences of log-likelihoods between trained Bernoulli-MCA (B-MCA) models and ground-truth parameters for bars test datasets. Average active number of bars  $\pi H$  is set by different prior probabilities  $0.2 \leq \pi \leq 0.5$  in steps of 0.05. Individual runs are shown with small offsets along the  $\pi$ -axis for better visualization. Percentages refer to the fraction of trained B-MCA models with higher log-likelihoods than the B-MCA models used to generate the dataset.

highly reliable approach to extract all bars for binary data (compare [90, 88]).

#### B.4 Natural Image Patches

The complete dictionary mentioned in Sec. 4.2 is depicted in Fig. 10.

#### B.5 Noise Type Estimation

The problem of noise type estimation has been addressed in a number of contributions. Teymura-zyan et al. [57] for instance studied the problem of distinguishing the type of noise in Positron Emission Tomography (PET) data [57]. In PET radioactive fluids are injected into humans or animals in order to obtain images for diagnostics or scientific studies. As a result, knowing the type of noise is crucial for different image processing routines [57, 91]. Other related work focused on machine learning automation (e.g., [58, 59]). In [58], a Bayesian approach is presented to infer the type of data in categories such as categorical, ordinal, count, real-valued, positive real-valued or interval. The algorithm does not directly suggest a likelihood model for the data, however. That is, for instance, it is still necessary to find out the best likelihood function that can fit positive real-valued data, e.g., Gamma, Inverse Gamma, Inverse Gaussian or an Exponential distribution. Vergari et al. in [59] further attempt to improve these results and aim to also infer the parametric likelihood model of the data. The approach is then shown to be more robust in working with missing, corrupted or anomalous data.

#### B.6 Denoising

We used images with gray scales in the interval  $[0, 255]$ . In order to rescale images to smaller intervals, we divided the data by its maximum and then multiplied the results by the desired peak value. We then employed the ef-MCA algorithms with  $H = 512$  and  $D = 12 \times 12$ . Each algorithm was trained once for 1000 EM iterations without any annealing procedure or any further processing on the data. For both E- and P-MCA algorithms, we manually set the minimum value of the  $W$  matrix to  $10^{-4}$  after each M-step updates in order to avoid zero values. We also employed the same sliding window averaging technique as in [51] and used 60 variational states.



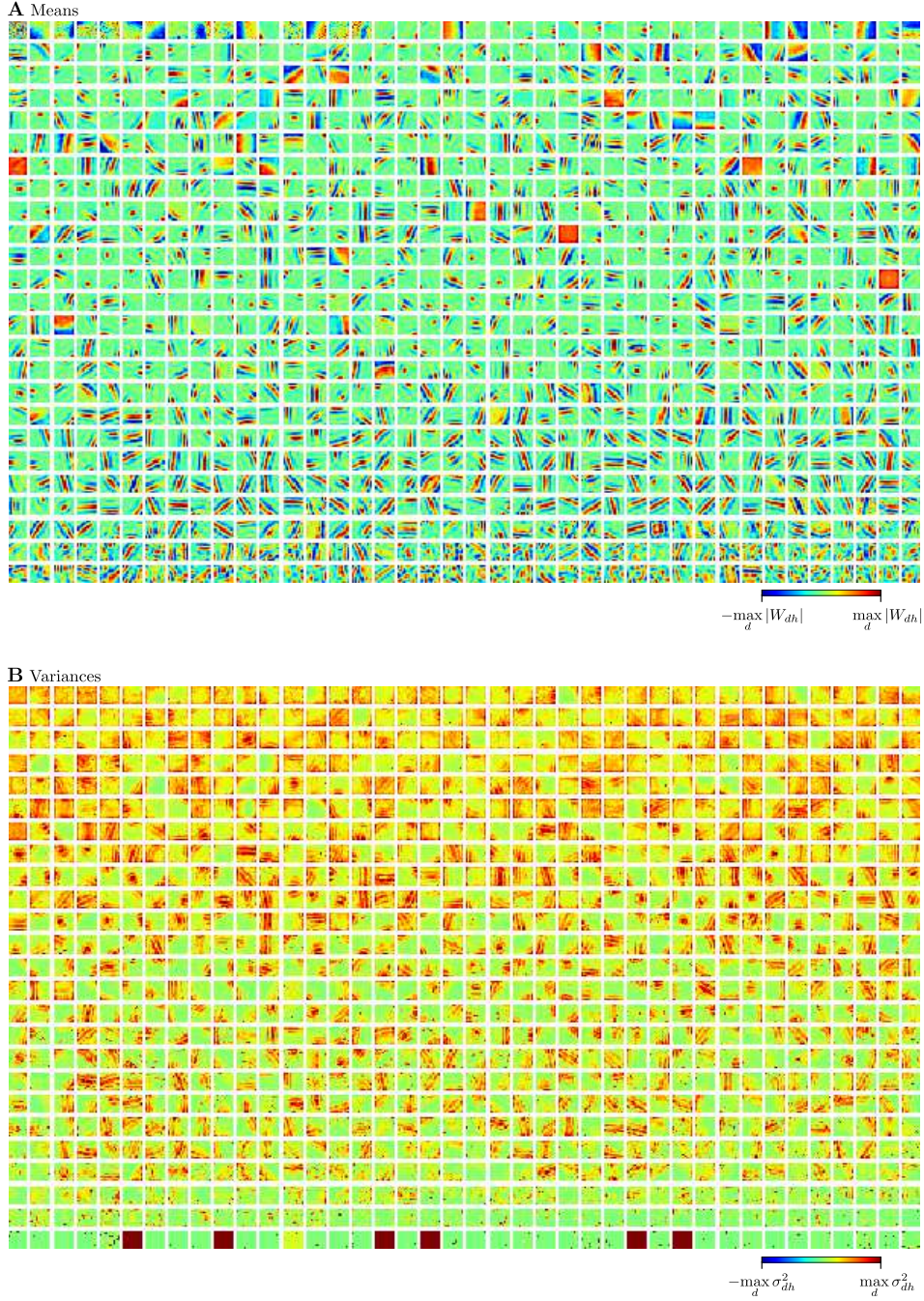


Figure 10: Complete dictionaries with  $H = 1,000$  component means and component variances learned from natural image patches using a Gaussian-MCA model (compare Sec. 4.2). The generative fields are ordered according to their activations, starting with the fields corresponding to the most active hidden units.

In addition, to apply the VST+BM3D model, we used the Anscombe transformation given by:

$$f : z \longrightarrow 2\sqrt{z + \frac{3}{8}} \quad (71)$$

and performed the BM3D algorithm with unit variance. The estimated, non-noisy image was then

transformed back using the inverse transformation (see, e.g., [74, 78] for further details):

$$f^{-1} : x \longrightarrow \left(\frac{x}{2}\right)^2 - \frac{3}{8}. \quad (72)$$